2008

Improved Structural Health Monitoring Using Random Decrement Signatures

Oleg V. Shiryayev
Wright State University

IMPROVED STRUCTURAL HEALTH MONITORING USING RANDOM DECREMENT SIGNATURES

A dissertation submitted in partial fulfillment
of the requirements for the degree of
Doctor of Philosophy

By

OLEG V. SHIRYAYEV
B.S.M.E., Wright State University, 2002
M.S.E., Wright State University, 2003

2008
Wright State University

WRIGHT STATE UNIVERSITY

SCHOOL OF GRADUATE STUDIES

March 27, 2008

I HEREBY RECOMMEND THAT THE DISSERTATION PREPARED UNDER MY SUPERVISION BY Oleg V. Shiryayev ENTITLED Improved Structural Health Monitoring Using Random Decrement Signatures BE ACCEPTED IN PARTIAL FULFILLMENT OF THE REQUIREMENTS FOR THE DEGREE OF Doctor of Philosophy.

Joseph C. Slater, Ph.D., PE
Dissertation Director

Ramana V. Grandhi, Ph.D.
Director, Engineering Ph.D. Program

Joseph F. Thomas, Jr. , Ph.D.
Dean, School of Graduate Studies

Committee on Final Examination

Joseph C. Slater, Ph.D., PE

Kuldip S. Rattan, Ph.D., PE

Junghsen Lieh, Ph.D.

J. Mitch Wolff, Ph.D.

Nathan W. Klingbeil, Ph.D.

Richard G. Cobb, Ph.D.

ABSTRACT

Shiryayev, Oleg. Ph.D., Department of Mechanical and Materials Engineering, Wright State University, 2008. *Improved Structural Health Monitoring Using Random Decrement Signatures*

Detection of structural damage phenomena such as cracks, delaminations, or loose fasteners is important because it increases safety and may allow significant reduction in operational costs. Many structural health monitoring techniques are based on detecting changes in vibration features obtained from the measured response. The technique presented in this work is based on the random decrement signatures calculated from the random response. No knowledge of input signal is required. Random decrement signatures have been used for damage detection purposes in the past. The significance of this work is that it explores the possibility of identifying the type of damage and focuses on detection of opening and closing cracks. Statistical features of the signatures are used to detect the presence of nonlinearity that often occurs due to onset of damage.

A numerical study was performed where simulated measurements were obtained from a finite element model of a frame containing a damaged member. The results of this numerical study showed that the new technique is able to detect crack type damage in a complex structure. It was able to highlight the damaged spar, but it was not able to precisely locate the damaged member in the spar. The results suggest that reliability of damage detection depends on the amount of noise in the measurements.

Experimental validation was performed using a cantilever beam experiment. The damaged beam used in the experiment contained a real fatigue crack instead of saw cuts that

are often used to simulate damage. The technique was shown to be able to detect damage when excitation level was greater than 1.0g RMS. The exact location of damage is not always detected reliably, as sometimes a segment of the structure adjacent to the actual damaged segment is indicated. The advantage of the new technique is that it is model-free and could be used on structures excited by ambient forces that are difficult or sometimes impossible to measure.

Contents

List of Figures

List of Tables

List of Symbols

β	stiffness reduction coefficient
$\Delta D_{xy}(\tau)$	difference RD function
$\hat{D}_{XX}(\tau)$	estimate of auto RD function
$\hat{D}_{XY}(\tau)$	estimate of cross RD function
σ	standard deviation
$\tau = t - t_i$	time passed the triggering time t_i
$E(\dots)$	expected value operator
k_d, k_h	damaged and healthy stiffness values
N	number of triggering points
$T^G_{X(t)}$	general triggering condition
$x(t_i + \tau)$	time segments used in averaging
$y(t_i + \tau)$	time segments used in averaging

Acknowledgement

Support for this work was provided by the Wright State University Graduate Council Scholar Fellowship and the Ph.D. in Engineering Assistantship. I want to thank my advisor Dr. Joseph Slater for guiding me through the laborious dissertation journey, and all other faculty who agreed to sacrifice their time and serve on my dissertation committee. I would also like to acknowledge Dr. Nathan Klingbeil for provision of computational resources, as well as Mr. Greg Wilt and Mr. Steve Page who helped me to accomplish experimental part of this work. Finally, I would like to thank my family who supported me during all those years in school.

Chapter 1

Introduction

In this chapter, common structural health monitoring (SHM) methods are discussed. The majority of SHM methods are based on detecting changes in the dynamics of the structure based on its vibration features. Those features are often used in conjunction with numerical models of structures to identify and locate the damage. Many methods for modal parameter estimation require knowledge of both input and output signals. However, in many situations measurement of system inputs are difficult to obtain, e.g. for structures with ambient excitation: buildings, bridges, or aircraft. This brings up the motivation for the use of the random decrement technique. A short description of the technique is provided.

1.1 Overview of structural health monitoring

Aerospace, civil, and other types of structures degrade during their service life. Degradation is usually comprised of cracking, delamination, or fastener loosening. Timely identification of structural damage is crucial for safety reasons. A multitude of vibration-based

approaches were developed over the past years. Worden and Dulieu-Barton [1] presented a hierarchical classification for SHM methods listed below. In this classification each consecutive level implies inclusion of the previous one.

1. *Detection*: the method provides a numerical indication that the damage has occurred.
2. *Localization*: the method provides information about a possible location of the damage.
3. *Classification*: the method provides information about the type of damage.
4. *Assessment*: the method is capable of estimating the severity of the damage.
5. *Prediction*: the method includes a capability to estimate the remaining useful life of the structure.

Development and practical implementation of accurate and efficient SHM methods involves a number of issues depending on particular applications. Those include and are not limited to selection of physical quantities to be measured, features used for SHM, quantity of sensors and their location, data processing, and robustness of the method to fluctuations in environmental conditions. This section provides a general overview of structural health monitoring and lists a variety of different approaches.

Doebling et al. [2, 3] provide an extensive literature review on damage identification based on modal properties. Also, another report by a group of authors [4] contains an extensive review of SHM related literature that was published in the period since 1996 until 2001. Carden and Fanning [5] presented a more recent literature review in 2004.

Detection of damage is commonly based on modal features such as resonant frequencies, damping ratios, and mode shapes. Since modal features are relatively sensitive to changes in the structure, detection functionality is usually the simplest one to implement.

- Modal-based methods

  It is observed that changes in natural frequencies can indicate a presence of damage. However, obtaining information about the location of damage by tracking changes in the natural frequencies is not trivial. Dilena and Morassi [6] presented a method for estimation of damage location based changes of resonant and anti-resonant frequencies for discrete dynamic systems. SHM methods that consider changes in the mode shapes or mode shape curvature can also provide information about the location of damage. Usually, measurements of higher modes are required to obtain information about the location of the damage.

  As an example of recent work, Bodeux and Golinval [7] fitted ARMAV time series models to identify the natural frequencies of a lab structure and detect the damage based on the changes in natural frequencies. Kim et al. [8] derived and compared methods for detection and location of damage in beam structures based on identified natural frequencies and mode shapes. Comparison of the methods was performed on FEM simulation data. The authors concluded that mode shape based method allowed for more accurate determination of damage location.

  Humar, Bagchi, and Xu [9] performed a study on reliability and accuracy of several modal-based SHM approaches through numerical studies. Models of three different structures were considered: a three-story shear frame, a bridge girder, and a space

truss. The following methods were included in the study: 1) Mode Shape Curvature Method [10], 2) Method Based on Changes in Flexibility Matrix [11], 3) Method Based on Change in Uniform Flexibility Shape Curvature, 4) Damage Index Method [12], 5) Method Based on Modal Residual Vector (e.g. [13]), and 6) Matrix Updating Methods. The authors indicated some drawbacks of those methods and concluded that they could fail to detect the damage under certain conditions. According to the authors, the Damage Index Method based on comparison of modal strain energy in the baseline and damaged states was the most promising. Errors in identification of damage were mostly attributed to the limited number of available measurement locations and errors in the measurements due to noise.

In order to be efficient and accurate, SHM procedures should be robust to operational and environmental fluctuations. Catbas, Brown, and Atkan [14] reported difficulties in modal parameter estimation of a bridge due to temperature variations. The changes in modal properties due to environmental fluctuations were as large as those caused by the controlled damage applied to the bridge. A literature review from Los Alamos National Laboratory [4] refers to a number of papers that investigate the effects of environmental changes on vibration signals of structures under investigation. Sohn et al. [15] indicate that the first natural frequency of the Alamosa Canyon Bridge varies as much as 5% due to temperature variation during a 24 hour period. The authors proposed the use of a linear filter to model the changes in the frequencies during the day.

- Methods based on matrix updating techniques

Matrix updating methods are another class of SHM techniques. These methods are based on computing perturbations to the baseline matrices using the measurement data. Essentially, the methods are formulated as optimization problems based on the equations of motion, baseline model matrices, and measured data. The differences between algorithms can be in formulation of the objective function, constraints, or numerical implementation of optimization algorithm.

Some SHM methods are concerned with monitoring changes in dynamically measured flexibility or stiffness matrices. The unity check is applied to verify the pseudoinverse relationship between the measured flexibility matrix and baseline structural stiffness matrix. Changes in the stiffness matrix were computed and correlated with the location of damage by Bedewi and Yang [16]. Similarly to stiffness matrices, mass and damping matrices can also be computed and used for SHM purposes. Siringoringo and Fujino [17] developed a method capable of detecting and locating loosened bolts in clamped steel plates with a lap joint. The method is based on computing the changes in the mass and stiffness matrices based on the changes in the state space system matrices obtained using the ERA technique [18].

- Neural networks based methods

Neural networks were found to be very useful for mapping purposes in various engineering fields. Depending on the architecture and the size of the network it is possible to train the network to be able to represent extremely complex nonlinear mappings. Doebling et al. [2] describe a number of papers that utilized neural networks in detection, location, and estimation of the extent of the damage. In general, the methods

are able to detect the damage, but they are not very accurate for finding the location and estimation of damage severity.

Another disadvantage of neural network based methods is that the many of them require a priori knowledge of the system model to generate training data from different damage scenarios. For large systems, the overall number of possible damage scenarios is usually also rather large, which results in large training data sets. Large training data sets are known to cause convergence problems and could lead to low accuracy of identification.

Recently Worden [19] proposed an SHM method based on novelty detection using neural nets that does not require a system model. The author reported successful results from numerical studies on a 3-DOF spring-mass-damper system. The damage was considered as a reduction in one of the spring elements. Transmissibility function computed between two masses served as the input vector to the neural network. The method was able to detect stiffness changes on the order of a few percent depending on the amount of noise present in the data.

Masri et al. [20] trained the network to map the input to the response of a nonlinear system in the reference state, while the damage indicator was based on the difference between the measured states and the states predicted by the network. Zapico, Worden, and Molina [21] used neural nets to detect and locate the damage in the two storey steel frame. The authors report that the network was only able to detect and locate the damage at the floor level, while it was not possible to locate stiffness degradation at the ends of individual longitudinal beams. Yeung and Smith [22] developed

a neural network based method to detect damage and tested it using simulation data from an FEM bridge model. Manson, Worden, and Allman [23, 24, 25] reported successful application of neural network based method for health monitoring of aircraft wing structures. Crupi, Guglielmino, and Milazzo [26] applied neural networks for detection of damage in rotating machinery.

- Nonlinear dynamics for structural health monitoring

  A vast majority of the methods reviewed by Doebling et al. [2] are based on the assumption of linearity of the studied structures and damage that occurs. However, not all real-world damage scenarios are a matter of linear stiffness reduction. In many cases structural changes are such that they result in nonlinear responses. For example, cracked beams are often modeled as structures with bilinear stiffness characteristics. Therefore, an ideal SHM solution should be capable of dealing with both linear and nonlinear types of damage effects.

  Recently, some research efforts are directed into exploiting nonlinear dynamics approaches and phenomena for SHM. Hunter [27] applied canonical variate analysis (CVA), which is essentially an ARMA based time series approach, to characterize a system with bilinear stiffness characteristics. Linear models were identified for different response regions. The authors were able to detect changes in the identified natural frequencies and mode shapes based on the obtained models. Epureanu and Yin [28] developed a technique based on detecting changes in the probability density functions of sampled attractors and applied it to a nonlinear aeroelastic system. Adams and Nataraju [29], and Brown and Adams [30] proposed the use of nonlinear

low order state space models for damage variables in order to facilitate prognosis of the state of the structure.

Nichols et al. [31, 32] investigated the use of attractor dimension as a feature for SHM. Moniz et al. [33] and Todd et al. [34] monitored the changes in the attractor formed from exciting the system by the output of a Lorenz oscillator. The assumption is that the system in a healthy state is a linear filter, while changes in the system (being linear or not) would cause the changes in the attractor.

Chen et al. [35] studied degradation of reinforced concrete beams and discovered that their dynamic behavior was close to that of a Duffing oscillator with softening stiffness. The authors developed a damage indicator based on the difference between the resonant frequencies obtained from dynamic tests with increasing and deceasing excitation frequency. Wang, Ren, and Qiao [36] defined a damage indicator based on coherence function that is sensitive to the onset of nonlinearity. The authors successfully detected damage in a steel frame.

- Smart materials in structural health monitoring

  It should also be noted that some recent works in the SHM field utilized smart materials for sensing and actuation. Mickens et al. [37] utilized PZT patches for sensing and excitation and compared the measured FRFs to distinguish between the healthy and damaged states. Park et al. [38] also used PZT patches in their work. They investigated an approach where an ARX model is fitted to predict the impedance measurements in the healthy state, while the difference between the predicted and the measured values would indicate the damage. In many practical situations the use

of PZT or other smart materials allows one to monitor and actuate remote areas that are difficult to access otherwise. Park et al. [39] proposed the use of piezoelectric sensors for SHM of structures subjected to high temperatures. Variations in impedance measurements due to controlled damage were observed to be significant with respect to the baseline data, making the proposed method quite appealing.

A number of publications describe SHM techniques based on propagation of ultrasonic waves excited by piezoelectric actuators. Those methods are typically aimed for detection of small localized defects. Mal et al. [40] used damage correlation factor based on system response vectors to identify delamination damage in a composite plate. Rizzo and di Scalea [41] used guided ultrasonic waves to detect notch defects in the cable strands used in civil structures. The damage indicator was defined as the ratio of the feature from reflected signal to the feature of direct signal. The results indicated that statistical features obtained from wavelet coefficients are more effective than those extracted from time or frequency domain features. Interested reader can find a large number of articles describing methods based on ultrasonic waves in relevant literature.

- Other approaches

Besides the various publications and methodologies mentioned above, numerous other approaches were developed. Sawyer and Rao [42] proposed the use of fuzzy logic theory in SHM. Fuzzy rules for detection and location of damage were developed based on results of FEM simulations. The authors demonstrated application of their technique on a numerical model of a cracked beam. Sampaio, Maia, and

Silva [43] proposed the use of the curvature of the FRF itself as a feature for damage detection. The authors tested the new method using the data from the simulation of a 10-DOF lumped mass system and experimental data from I-40 bridge across Rio Grande in Albuquerque, NM, USA.

Ismail, Razak, and Rahman [44] developed another technique based on changes in curve-fitted mode shapes to detect and locate the damage in reinforced concrete beams. Maia et al. [45] compared the mode shape based methods and FRF based methods. The authors report that curvature based methods generally perform better, although they are more susceptible to false alarms.

Sohn et al. [46] applied extreme value statistics to the novelty index obtained from neural network outputs. Novelty-based damage detection requires assigning a certain threshold value for the index to be the decision boundary for damage detection. In order to improve the accuracy of damage detection, extreme value statistics are applied. Sohn and Law [47] applied Bayesian framework for SHM based on the Ritz vectors, arguing better detection results than with the direct use of modal vectors. However, in order to implement this approach, a database of failure scenarios has to be available. Castro, Garcia-Hernandez, and Gallebo [48] utilized features obtained from wavelet transform of displacement signal to detect and locate the damage in rods. Also, Reda Taha et al. [49] provided an overview of the usage of wavelet transform and features based on it for structural health monitoring.

There have been some attempts to develop techniques that would allow real-time health monitoring of structures. Vanlanduit, Verboven, and Guillaume [50] proposed

a technique for on-line monitoring of system poles and demonstrated it on a beam with a propagating fatigue crack. Yang, Lei, Lin, and Huang [51] applied empirical mode decomposition technique and Hilbert-Huang transform to detect damage events that occurred during the data acquisition process. The authors used simulated data from a numerical model of a building structure. The technique was able to detect the time instants when the damage event occurred by monitoring changes in the natural frequencies.

All vibration based SHM methods can be divided into two general classes: those that require a numerical model of the structure under investigation, and those that do not require having such a model. For example, many matrix updating methods are developed with the assumption that an FEM model of the structure is available. Implementation of such a technique will typically require tuning of the model in order for it to be able to replicate the response of the structure in the healthy state. Obviously, for simplicity reasons, it is advantageous to have an SHM method that does not require a numerical model of the system or extensive a priori knowledge about the system. On the other hand, it is practically impossible to develop a method capable of level 3 and higher identification without any information about the system.

Another family of SHM techniques is based on the use of Random Decrement (RD) signatures. The concept of the RD technique was introduced by Henry Cole in early 1970s [52, 53, 54]. He was trying to develop a reliable method for estimation of damping in the aerospace structures subject to ambient excitation [55], which was based on autocorrelation functions. The new technique proposed by Cole was based on time averaging of the ran-

dom response. The resulting randomdec signatures are very sensitive to the changes in the structure, so Cole proposed their use for damage detection. In particular, he noted visible differences between the baseline signatures and the signatures from the structure with loose bolts. Also, he documented significant changes in the RD signatures during a wind tunnel test of a wing model prior to its failure.

Among the advantages of using RD signatures for SHM is that no input measurements are necessary. The technique proposed by Cole was also applied for damage detection of civil structures. More detailed description of SHM techniques based on RD method is given in Chapter 2. The techniques using RD method that were developed up to date can detect, and some of them can also indicate, a likely location of damage if the system model is available. However, no research was done attempting to detect and locate the damage based on the changes in RD signatures without using an analytical system model of some sort. The proposed method will not require a numerical model of the system or generation of extensive databases of damage scenarios. Identification of damage and its location is proposed to be based on certain statistical features of the signatures. The randomdec technique is introduced next.

1.2 The concept of the Random Decrement technique

The concept of RD technique is relatively simple and it is not very difficult to implement this technique numerically. Following the reasoning of Cole, the random decrement function $\hat{D}_{XX}(\tau)$ can be estimated as the average of the time segments $x(t_i+\tau)$ of the response,

and the starting point for each segment is when the displacement reaches a certain value $x(t_i) = a_0$, shown in equation (1.1)

$$\hat{D}_{XX}(\tau) = \frac{1}{N}\sum_{i=1}^{N}\{x(t_i+\tau)|x(t_i) = a_0\} \tag{1.1}$$

In this equation, the estimate of the RD function $\hat{D}_{XX}$ is a function of time variable $\tau = t - t_i$, which represents the time past the triggering time t_i, N is the number of triggering points, and $x(t_i) = a_0$ is referred to as the triggering condition. However, in reality the measurements are only available in discrete form, hence the probability of response measurements taking an exact value $x(t_i) = a_0$ is near zero. To avoid this problem, a level crossing triggering condition is implemented. This defines the triggering point to be the measurement point at which the displacement becomes larger or smaller than a certain value. In a more general form, equation (1.1) can be rewritten as shown below

$$\hat{D}_{XX}(\tau) = E(x(t_i+\tau)|T^G_{X(t)}) \tag{1.2}$$

where $T_{X(t)}$ is the triggering condition. The choice of the triggering condition for the RD technique is left to the user. A formally sound definition of the triggering conditions is due to J. C. Asmussen [56], who proposed it as

$$T^G_{X(t)} = \{a_1 \leqslant X(t) < a_2,\ b_1 \leqslant \dot{X}(t) < b_2\} \tag{1.3}$$

It is important to note that the RD function defined by equation (1.2) is referred to as the *auto* RD function. This is denoted by subscript XX, which implies that only single channel measurement is considered. In late 1970s Ibrahim [57] introduced a concept of *cross* RD functions, which allowed application of the RD technique for identification of mode shapes. Using a general triggering condition, the estimate of the cross RD function

is defined as

$$\hat{D}_{XY}(\tau) = \frac{1}{N}\sum_{i=1}^{N}\{y(t_i+\tau)|T^G_{X(t)}\} = E(y(t_i+\tau)|T^G_{X(t)}) \tag{1.4}$$

To illustrate the RD technique, displacement data from a linear single degree of freedom (SDOF) system excited by white noise is considered. In Figure 1.1, the level crossing triggering condition is chosen to be $T_{X(t)} = \{x(t_i) = 1.5\sigma_x\}$. The subfigures indicate the averaging process, and the estimated RD function. In the case shown, the time history is very short and there are only 6 triggering points used in the estimation process. In order to obtain reasonable estimates many more response segments have to be used in the averaging process. Besides the number of sampled segments used in the estimation, there are other factors that affect the accuracy of estimated RD function. In his dissertation Asmussen [56] provides theoretical details about estimation of random decrement functions.

A few words have to be said about the applications of the RD technique. The original application of the technique as proposed by Cole was damage detection and damping estimation in aerospace structures excited by ambient forces. The technique has later been used for modal parameter estimation and linear system identification in cases where input measurements were not available and it was reasonable to assume random Gaussian inputs. Cho et al. [58] used the technique to estimate damping in industrial towers and chimneys. Asmussen [56, 59, 60] applied the technique for modal analysis of bridges subject to random excitation from the traffic. The technique was also applied for damage detection in offshore structures [61, 62]. Chapter 2 contains more details concerning application of the technique for health monitoring of structures.

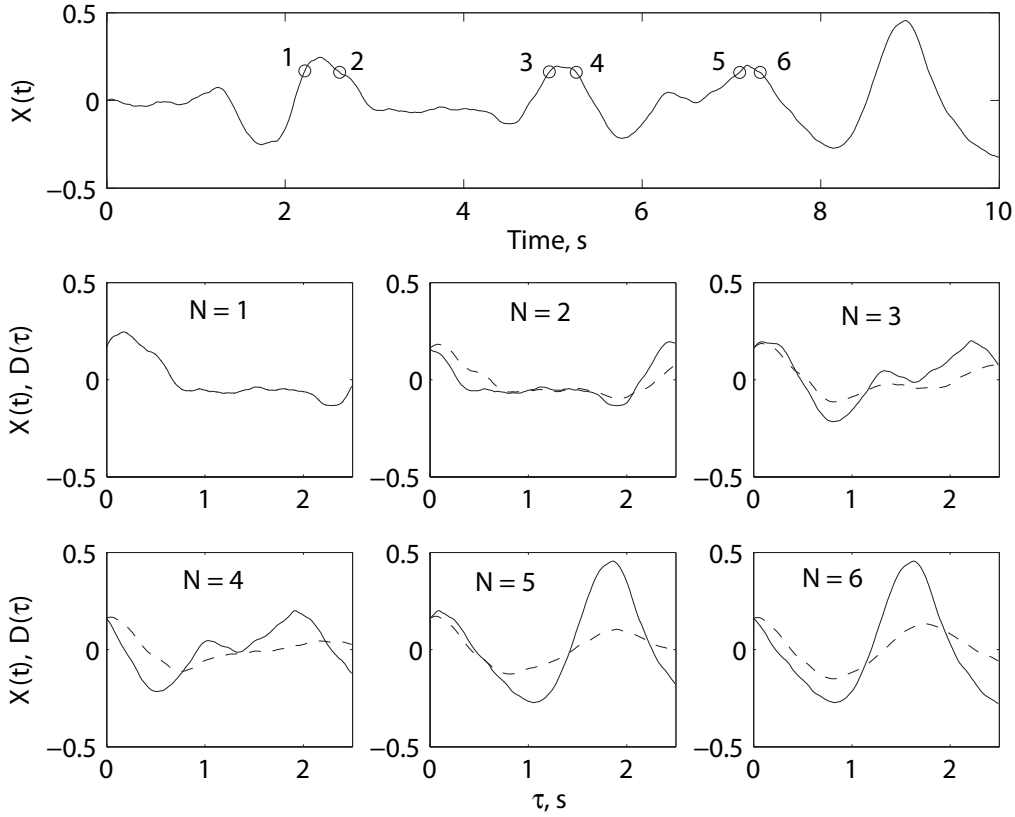

Figure 1.1: Displacement measurement data from SDOF system. Triggering points are designated with "o" marks. Estimated RD function – dashed line, picked response segment – solid line.

1.3 Overview of this work

Chapter 2 discusses previous applications of RD technique for structural health monitoring and introduces the new health monitoring approach based on RD signatures. A study of a 5 DOF system is presented to describe the procedures used to obtain the features that are utilized for detection, location, and classification of the different types of nonlinearities. Chapters 3 and 4 present application of the new technique to the data from the finite element model of a wing-like frame structure. In that study, the damage was considered in the form

of an opening and closing crack in one of the structural members. Chapter 5 reports the results from application of the new method to experimental data from a cantilever beam. In this experiment the damage was in the form of a fatigue crack. Conclusions are presented in Chapter 6.

Chapter 2

Structural Health Monitoring Using Randomdec Signatures

2.1 Overview of previous work

Randomdec signatures change shape if a crack or some other flaw has developed and this fact can be utilized for damage detection. The baseline RD signature of the system is first estimated by averaging a sufficiently large number of RD signatures during the operation of the system in a reference healthy state. A region is defined about the baseline signature based on desired the confidence level to reject false alarms. If current signatures start to fall out of the specified baseline region, the decision is made that the damage has occurred. This approach was used by Cole [54].

A different approach was applied for health monitoring of the offshore structures by Yang et al. [61]. They considered the damage indicator to be the mean square deviation of

the current signature from the baseline signature expressed as

$$\text{MSD} = \frac{1}{N}\sum_{i=1}^{N}\left[D_1(\tau_i) - D_2(\tau_i)\right]^2 \tag{2.1}$$

where $D_1(\tau_i)$ and $D_2(\tau_i)$ are the data points from two signatures from the same time lag τ_i, and the total number of points in the signature is N. The authors found that the magnitude of the damage metric increased substantially in cases when damage was present in the structure. This damage metric is suitable for detection of damage, but it does not allow to locate the damage.

Tsai, Yang, and Chen [62] used the RD technique to identify damage in a scaled model of an offshore platform. Damage was in the form of a saw cut to one of the structural members. Natural frequencies and damping ratios were obtained by curve-fitting autoregressive models to the RD signatures obtained from several accelerometers. The damage was identified by monitoring changes in the modal properties. The authors correlated significant changes in the phase of the highest identified mode with the location of the damage. Hence, the technique proposed by Tsai et al. can be categorized as level 2.

Bedewi and Yang [63, 16] proposed an SHM technique that relies on a system identification method, which was developed by the same group of authors. The technique uses RD signatures to estimate the mass, stiffness, and damping matrices of the system under the assumption of linearity. The damage in the structure was introduced by a through cut in one of the members. The authors found that with the onset of damage, diagonal elements of the stiffness matrix do not change much, but off-diagonal elements undergo significant changes allowing one to identify the location of the damage.

The RD technique was also applied to monitor damage in ship structures by Zubaydi,

Haddara, and Swamidas [64]. The authors compared the RD signature to the free response obtained from a finite element model of a stiffened plate representing part of the ship's hull. The damage was considered to be in the from of saw cuts of different lengths. It was demonstrated that the signature changed significantly depending on the cut length. In their later work [65] the authors created a finite element model of the ship's side shell and trained a neural network to obtain a damage indicating function. This approach allowed detection and location of damage.

Li et al. [66] studied the RD signatures obtained from a fiber reinforced composite beam. The authors considered the damage to be in the form of localized delamination. It was found that the frequency of the fundamental mode decreases while its damping ratio increases with an increase of delamination length. The authors proposed generation of a database of signatures for the system using known failure scenarios. Then, use a pattern recognition technique such as neural networks to identify and classify the damage. However, they reported significant differences between the experimental signatures and those obtained from the numerical model. The main drawback of this approach is that it requires building very accurate numerical model of the structure. But building an accurate model is a great challenge due to complexities involved in accurate modeling of damping mechanisms, vibration exciters, instrumentation attached to the structure, and accurate representation of boundary conditions.

To summarize the above, some of SHM methods utilize RD signatures themselves as damage indicators, while others utilize them as a tool for updating the model of the system and then use the changes in the model as features for damage detection. Another benefit

of using RD signatures is that excitation measurements are not necessary in order to obtain them. As of now, Randomdec-based SHM methods can achieve level 2 damage identification. The main goal of this work is to develop a basis for an RD-based SHM method that will allow detection and location of damage based on changes in statistics and will not require having a numerical model of the structure. Instead, for determining the location of the damage, connectivity between the DOFs will be considered. The description of the proposed methodology along with the results of preliminary investigations are presented next.

2.2 Proposed Approach

The proposed method relies on detection and classification of novelty in the RD signatures, and does not require identification of a system model. A schematic of the steps in the procedure is presented in Figure 2.1. The details of the procedure follow.

First, measurement data is obtained and RD signatures are calculated using the averaging process. In the feature extraction stage difference signatures $\Delta D_{xy}(\tau)$ are obtained. These are simply the difference between the signatures of the neighboring DOFs,

$$\Delta D^{ij}_{xy}(\tau) = D^{i}_{xy}(\tau) - D^{j}_{xy}(\tau) \tag{2.2}$$

where superscripts i and j denote the indices of the neighboring DOFs. Several statistics are calculated from the difference signatures. Those statistics are then compared to the baseline values obtained from the system in the healthy state and a decision is made whether the stiffness change is present and where it is located.

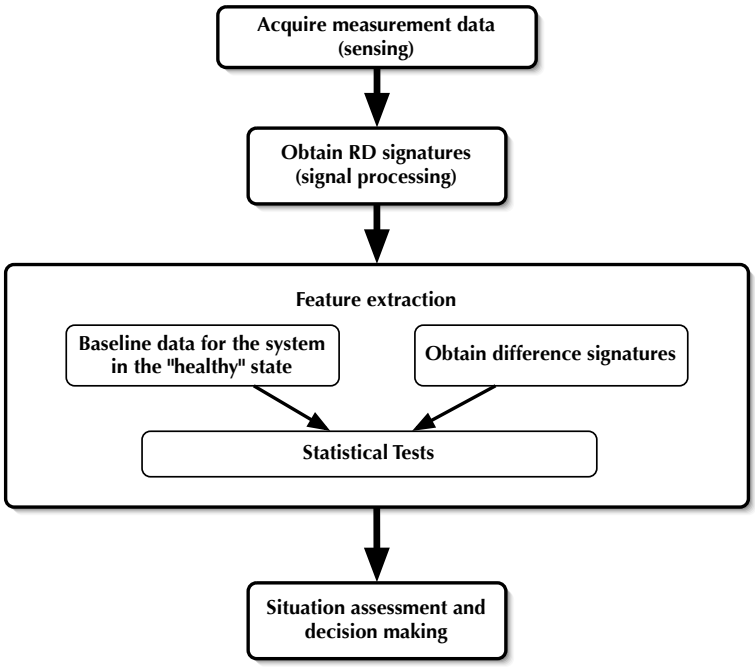

Figure 2.1: Flow chart for structural health monitoring procedure.

In order to characterize linear stiffness degradation, it is convenient to use energy based reasoning. Consider that the system in both healthy and damaged states is supplied the same amount of energy: $\frac{1}{2}k_h X_h^2 = \frac{1}{2}k_d X_d^2$, where subscripts h and d indicate healthy and damaged states of the system. Since it is common to collect acceleration measurements in testing, and acceleration is correlated with displacement, the ratio of the stiffnesses can be written in terms of the accelerations as

$$\frac{k_d}{k_h} \propto \frac{\ddot{X}_h^2}{\ddot{X}_d^2} \tag{2.3}$$

Instead of dealing with squared acceleration, we utilize standard deviations of the difference signatures since these quantities are related to the variance and therefore energy of the signal. It is proposed that the feature that can quantify linear stiffness degradation is

expressed as the ratio of standard deviation (STD) values of the respective signatures:

$$\text{STD ratio} = \frac{STD(\Delta D_{xy}(\tau))_{healthy}}{STD(\Delta D_{xy}(\tau))_{damaged}} \sim \frac{k_d}{k_h} \tag{2.4}$$

The other two tests performed in this study were concerned with comparing the means and the skewness of the signatures with respect to the baseline signatures. The difference of the means criterion is defined mathematically as

$$\text{Difference of the means} = \text{mean}(\Delta D_{xy}(\tau))_{healthy} - \text{mean}(\Delta D_{xy}(\tau))_{damaged} \tag{2.5}$$

The skewness difference criterion is defined as the ratio of the third ccentral moment and the cube of the sample standard deviation.

$$\text{Difference of the skewness} = \text{Skewness}(\Delta D_{xy}(\tau))_{healthy} - \text{Skewness}(\Delta D_{xy}(\tau))_{damaged} \tag{2.6}$$

where the skewness is obtained as

$$\text{Skewness} = \frac{E(x-\mu)^3}{\sigma^3} \tag{2.7}$$

Both of those criteria were chosen based on the sense that nonlinear changes in the system would change the distribution of the response and therefore affect those statistics of the signatures. Results from numerical studies are presented next.

2.3 Numerical Study of a 5 DOF System

The study was performed using a 5 DOF system shown in Figure 2.2. In the healthy state the system was considered to be linear and the parameters were set to be $m_i = 1$ kg,

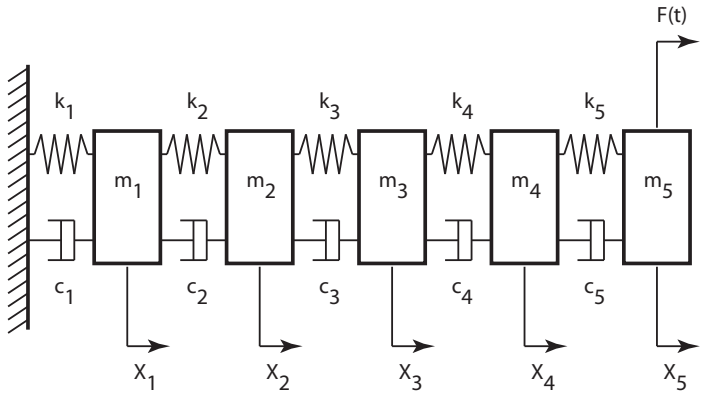

Figure 2.2: 5 DOF system.

$c_i = 1.9$ N/m·s, and $k_i = 17550$ N/m, $i = 1...5$. The above values were selected to generate a system with light damping, which is typical for aerospace structures. The modal parameters for the system in the healthy state are summarized in Table 2.1.

Mode	1	2	3	4	5
Natural frequency, Hz	6.0012	17.5174	27.6145	35.4744	40.4604
Damping ratio, ζ, $\cdot 10^{-3}$	2.0411	5.9579	9.3921	12.0654	13.7612

Table 2.1: Modal parameters for a 5 DOF system in healthy state.

Excitation to the system was applied at DOF X_5 in the form of Gaussian white noise with a variance of $\sigma_F^2 = 20000$ N^2. Acceleration measurements were used since they are commonly obtained in testing. Matlab [67] was used to integrate the equations of motion for the system. Simulations were performed using the Runge-Kutta $4^{th} - 5^{th}$ order method, and the length of random vibration time histories collected was 1000 seconds in all cases. The sampling rate was fixed at 0.002 seconds.

Level crossing triggering condition on DOF X_1 was used to obtain RD signatures. The triggering level was set at $1.5\sigma_{\ddot{x}_1}$. To establish baseline signatures, 30 data sets from the healthy system were obtained. The signatures obtained from each data set were averaged to obtain the baseline healthy signatures. This step is necessary since RD signatures have certain variability and the averaged signature would prevent an outlier being considered as a baseline signature.

Three types of stiffness changes were considered in the study: linear stiffness degradation, bilinear stiffness, and trilinear stiffness characteristic.

- Linear stiffness degradation (Figure 2.3(a)), $k_d = \beta k_h$, $0 < \beta < 1$.
- Bilinear stiffness (Figure 2.3(b)), $k_d = \beta k_h$, where $\begin{cases} 0 < \beta < 1, \ x \geqslant 0 \\ \beta = 1, \ x < 0 \end{cases}$
- Trilinear stiffness (Figure 2.3(c)), $k_d = \beta k_h$, where $\begin{cases} 0 < \beta < 1, \ |x| \leqslant d_{lim} \\ \beta = 1, \ |x| > d_{lim} \end{cases}$

where k_d and k_h are the stiffnesses of the damaged and the healthy spring elements, and β is the reduction coefficient. In the case of linear stiffness degradation, the stiffness of the spring is reduced throughout the entire range of displacements as shown in Figure 2.3(a). The bilinear stiffness characteristic as shown in Figure 2.3(b) is usually used to model structures with opening and closing cracks. Trilinear stiffness characteristic depicted in Figure 2.3(c) can be used to model slipping type behavior which can be found in jointed structures with loosened fasteners.

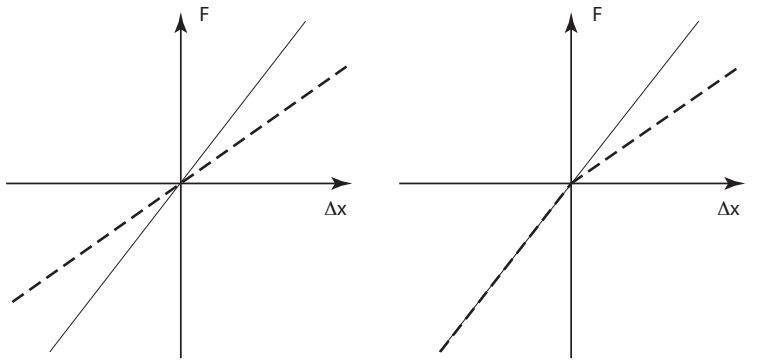

(a) Linear stiffness degradation. (b) Bilinear stiffness characteristic.

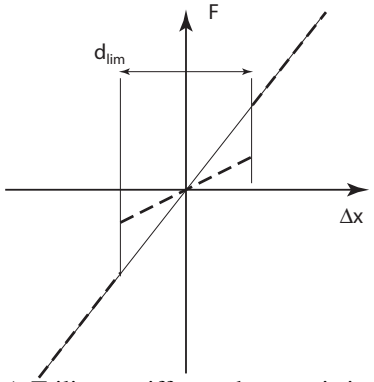

(c) Trilinear stiffness characteristic.

Figure 2.3: Spring stiffness characteristics. Solid - healthy state, dashed - damaged state.

First, we consider a case when spring element k_5 is damaged. This case would indicate a scenario when stiffness change occurs very close to the location of excitation and therefore should be detected most easily. In this case, for each of the three damage scenarios 3 levels of damage was considered, corresponding to $\beta = 0.9$, 0.7, and 0.5. Then, we consider cases when other spring elements are damaged to test the ability of the method to identify location of damage. In those cases, stiffness reduction coefficient was set to be $\beta = 0.5$.

2.3.1 Case when spring element 5 is damaged

Spring element 5 is chosen to assess the ability of the proposed method to detect stiffness changes in a situation when the damage site is located near the excitation source. Typically, changes in the dynamics of the structure are more pronounced when damage is located near the source of excitation. In such case the damage should be easily detectable, which would illustrate the performance of the method in an "ideal" situation.

Linear stiffness degradation

Figure 2.4 illustrates result from applying the STD ratio test to the data from a system with linear stiffness reduction. It is clear that the STD ratio criterion was able to successfully detect, locate, and even quantify the stiffness degradation in spring element 5 connecting DOFs 4 and 5. It must also be noted that due to the changes in the system, the criterion values for other DOFs vary significantly from their baseline conditions. Nevertheless, the largest variation is observed for the difference signatures between 4^{th} and 5^{th} DOFs.

Figure 2.5 depicts the values of the mean difference and the skewness criteria for the system with linear stiffness degradation. The skewness criterion shows a noticeable change for the difference signatures of DOFs 3-4 (spring element 4). The mean difference criterion does not show any significant changes for any of the difference signatures. Note that changes in the skewness criterion are significantly larger than those in the mean criterion.

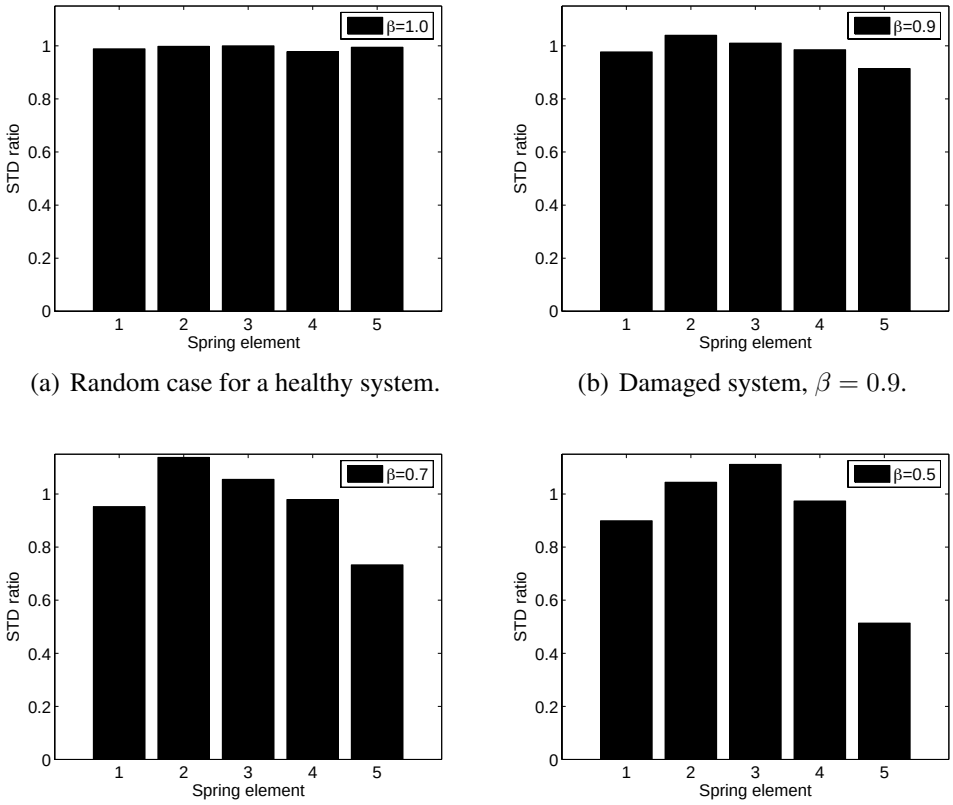

(a) Random case for a healthy system.

(b) Damaged system, $\beta = 0.9$.

(c) Damaged system, $\beta = 0.7$.

(d) Damaged system, $\beta = 0.5$.

Figure 2.4: Values of the STD ratio criterion for a system with various levels of linear stiffness degradation in spring element 5.

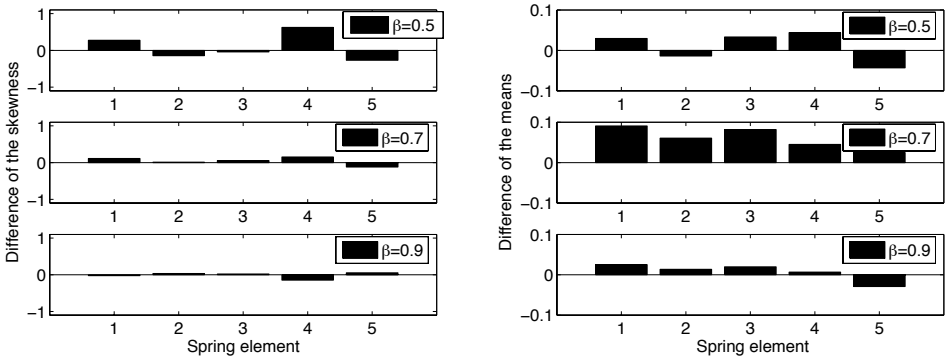

(a) Skewness test results.

(b) Difference of the means test results.

Figure 2.5: Difference of the means and the skewness tests for the system with linear stiffness degradation in spring element 5.

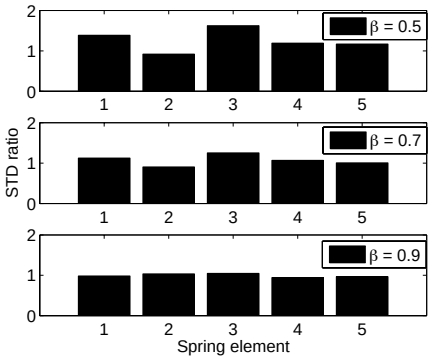

(a) STD ratio results.

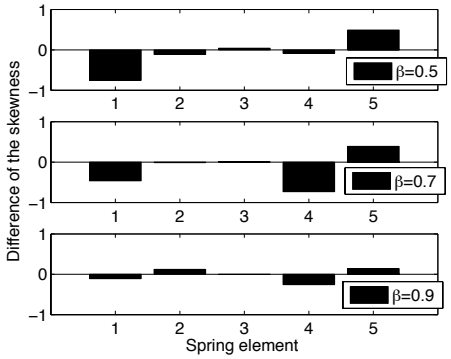

(b) Skewness test results.

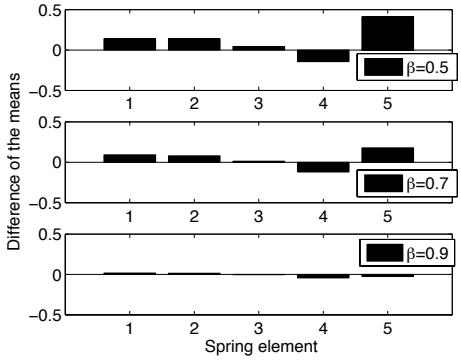

(c) Difference of the means test results.

Figure 2.6: Test results for the system with bilinear stiffness spring element 5.

Bilinear stiffness

From Figure 2.6 one may infer that the STD ratio test for the system with bilinear stiffness indicates increased stiffness at most DOFs. This conclusion may be drawn from the fact that the STD ratio was found to be greater than unity for the respective spring elements (see equation 2.4). It is not possible to locate the damage based on that test. The skewness test indicates significant changes at 1^{st} and 5^{th} DOFs. The mean difference test indicates significant change at the difference signatures between DOFs 4 and 5, allowing to locate the damage.

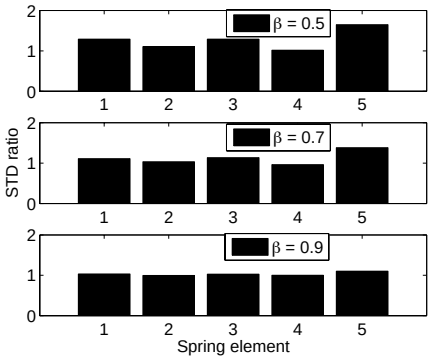

(a) STD ratio results.

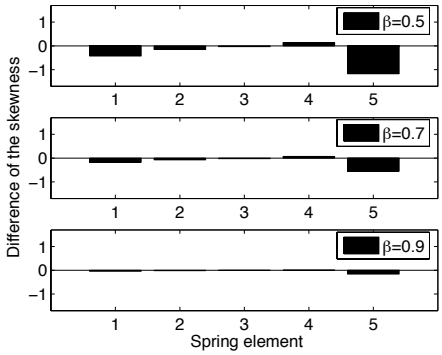

(b) Skewness test results.

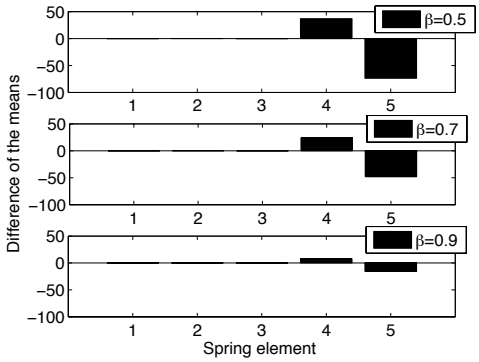

(c) Difference of the means test results.

Figure 2.7: Test results for the system with trilinear stiffness spring element 5.

Trilinear stiffness

From Figure 2.7, one can conclude that the STD ratio test indicates an increase of stiffness between DOFs 4 and 5, and a decrease between DOFs 4 and 3. The skewness test shows significant changes in the difference signatures between DOFs 5 and 4, and DOF 1 with respect to fixed reference. The most noticeable changes are shown by the test for difference of the means. As Figure 2.7(c) indicates, the means of the difference signatures between DOFs 5 and 4, and DOFs 4 and 3 have changed very significantly, while the means of the rest of the difference signatures did not change. Hence, one can conclude that the test for

the difference of the means is useful for identifying this type of stiffness change.

2.3.2 Cases with damage at spring elements 4, 3, 2, and 1

The ability of the proposed features to identify damage at other locations was studied by changing the characteristics of the other spring elements. In all cases the level of damage was considered to be $\beta = 0.5$ and excitation was kept at the same level as before and applied at mass 5.

Figure 2.8 contains the results of the STD tests for system with linear stiffness reduction at various DOFs. One can observe that for cases when the damage is located at DOFs 2, 3, and 4, the STD ratio criterion that has the largest change from unity corresponds to the difference signature of the damaged spring element. For the case when damage is located at spring element 1, it is not possible to draw a conclusion about the location of the stiffness change. It is speculated that the reason for this result is that excitation is applied at mass 5 away from the damaged element, so the damage has a relatively small effect on the system's response.

Figures 2.9 and 2.10 contain results of the difference of the means tests for systems with bilinear and trilinear stiffness elements in different locations. Clearly, in all cases the largest change is indicated for the difference signature that corresponds to the damaged spring element. Note that the for the cases with trilinear stiffness, the magnitude of the change indicated by the difference of the means test is significantly larger.

Figure 2.11 illustrates the results of the difference of the skewnesses test results for the

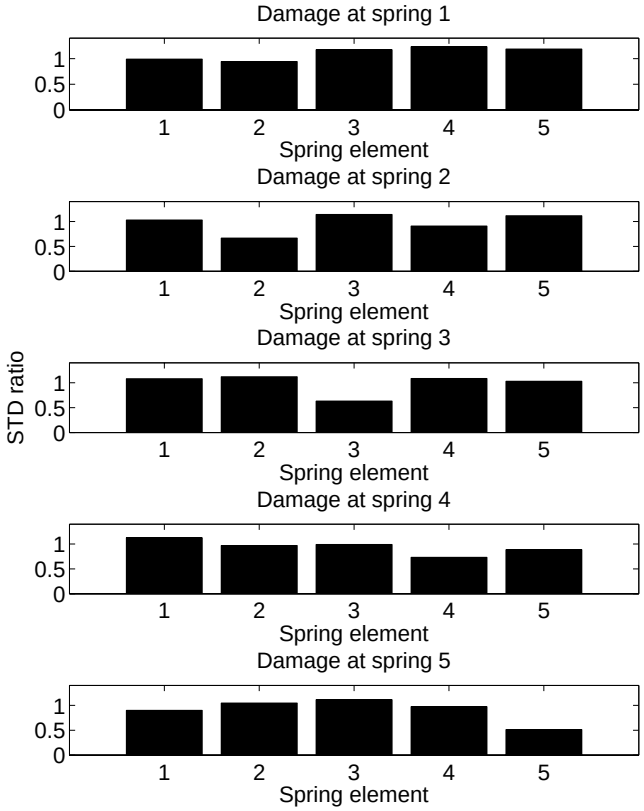

Figure 2.8: STD ratio test results for system with linear stiffness degradation.

case with bilinear stiffness degradation. Based on the results of this test it is not possible to identify the location of damage. Similar conclusion could be drawn from the results of the skewnesses tests from cases with other types of nonlinearities. Therefore, this test may not be very useful for identification of the location of the damage.

2.4 Summary and General Comments

Results of this preliminary investigation indicate that both the STD ratio test and the difference of the means test are useful for detecting and locating the damage. However, the test

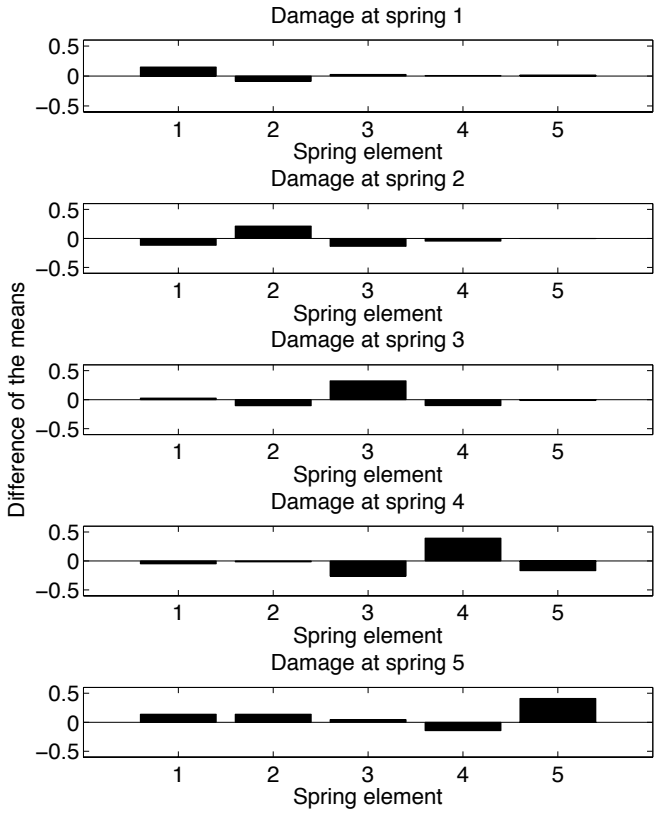

Figure 2.9: Difference of the means test results for system with bilinear stiffness degradation.

on the skewness statistic appears to be ineffective. Also, the results indicate that sensitivity of the tests decreases if the nonlinear spring element is located further away from the excitation source. In the case when input excitation is distributed across all DOFs it is expected that it will be easier to observe changes in dynamics, which will make damage detection more reliable. Although RD signatures were previously utilized for detection of damage, the significance of the idea presented here is that different statistical tests can be designed to target different types of damage. Hence, in the future it may be possible to create a complex RD-based SHM approach that will allow to detect different types of damage.

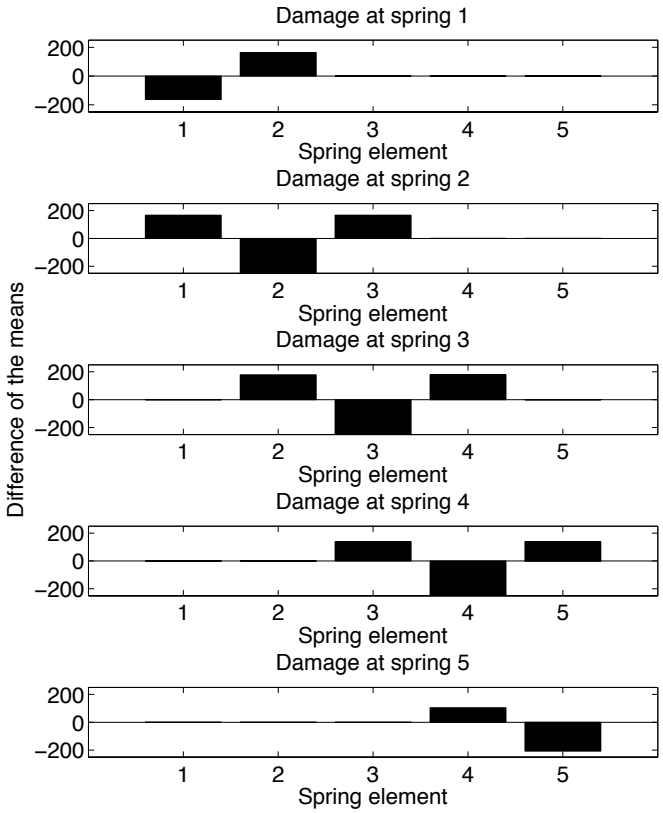

Figure 2.10: Difference of the means test results for system with trilinear stiffness degradation.

The following chapters of this dissertation are focused on identification of opening and closing cracks. Detailed studies encompassing detection of several different types of damage that were considered in this chapter would require a rather large amount of time and effort, greatly exceeding that suitable for a single dissertation.

Cracks are common precursors of fatigue failures. Detection of fatigue cracks has been given ample attention in the literature. For example, most of the works cited earlier in this chapter that utilized Randomdec signatures for SHM purposes considered the damage to be in the form of the crack.[62, 63, 16, 64] Also, a large number of other methods were

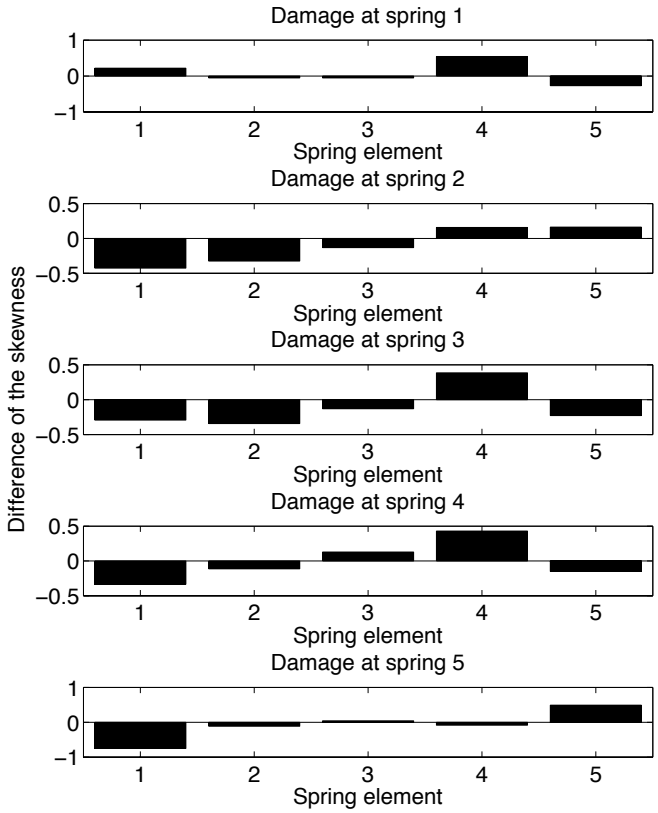

Figure 2.11: Difference of the skewnesses test results for system with bilinear stiffness degradation.

developed for crack detection [68, 36, 69, 70, 45, 47, 71, 72, 73, 74, 75, 76, 77, 78, 79]. In most of these works [68, 36, 69, 70, 45, 47, 71, 72, 73, 74, 75, 76] the crack is considered to be open and is usually introduced as a saw cut in the experiment.

This approach may not be very realistic. Real fatigue cracks introduce local flexibility into a structural member, but they are not always equivalent to saw cuts. Depending on the static load on the structure and the level of excitation, the cracks can remain always open, always closed, or they can open and close during vibration cycle. Considering fatigue cracks as open cracks and representing them as saw cuts in experiments essentially

assumes a reduction in structural stiffness, which remains a linear characteristic. Linearity assumption is usually made to stay away from the difficulty of dealing with nonlinearity introduced by opening and closing cracks.

Chondros, Dimarogonas, and Yao [80] showed both analytically and experimentally that changes in the natural frequencies for a cantilever beam with a breathing crack are much smaller than these for a beam with an open crack. Hence, SHM methods that carry the assumption of linearity are more suitable for detection of open cracks and are inherently less sensitive to the breathing cracks. Several works considered nonlinear characteristics that arise due to breathing cracks for damage detection [81, 78, 82, 83, 79, 77, 84]. However, randomdec signatures have not yet been utilized for detection of damage based on the onset of nonlinearity due to a breathing crack.

The primary contribution of this work is the detailed study on the detection of breathing cracks using randomdec signatures based on the onset of bilinear stiffness characteristic. The study of a 5 DOF system involved simple connectivity between DOFs, while real structures have a much more complex geometry. The proposed SHM methodology is first studied using a more complex system such as a space frame in the next two chapters. This study is performed on acceleration data from an FE model. The technique is then applied to the experimental data from a cantilever beam that contains a fatigue crack. Experimental results are presented in Chapter 5.

Chapter 3

Finite Element Model

3.1 FE Model

The technique of Chapter 2 is applied to the data obtained from the finite element model of a frame-like structure developed in Abaqus [85]. Figure 3.1 illustrates the geometry of the structure. The structure contains four longitudinal members fixed at the far end and five cross members. Each longitudinal member is represented by five beam elements employing quadratic formulation with rectangular hollow cross section (Figure 3.2(b)). Each cross member is represented by three quadratic beam elements with solid rectangular cross section (Figure 3.2(a)).

Structural members are assumed to be made of 7075-T6 aluminum, with the following properties: $\rho = 2810\ kg/m^3$, $E = 72\ GPa$, $\nu = 0.33$, $G = 26.9\ GPa$. The explicit central difference time integration scheme is used to calculate the dynamic response of the structure in ABAQUS. Preliminary analysis in ABAQUS estimated the stable time step to be $\approx 3.8 \cdot 10^{-7}$ sec. To ensure accuracy of direct integration a time step of $2 \cdot 10^{-8}$

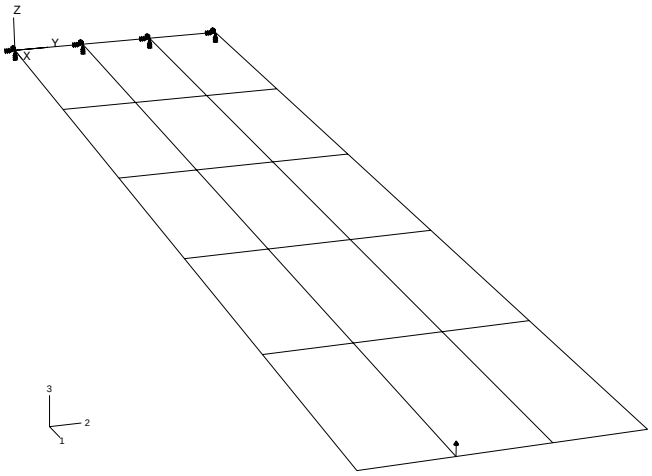

(a) Abaqus capture of the frame model.

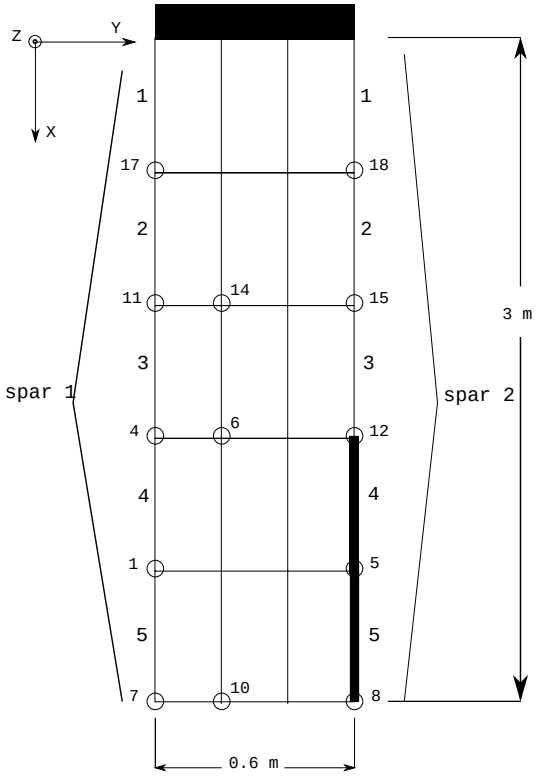

(b) Schematic of the frame model (top view). Segments highlighted in bold are considered for the two cases of damage.

Figure 3.1: 3-D frame structure.

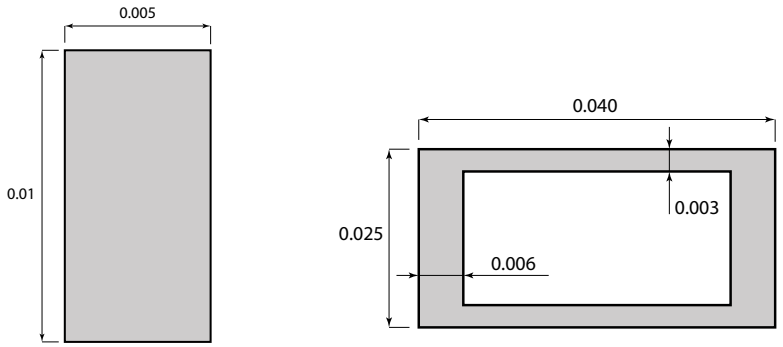

(a) Rib section, dimensions in meters.

(b) Spar section, dimensions in meters.

Figure 3.2: Cross sections of structural members (not to scale).

sec. is used in the FEM simulation. Presumed unknown band-limited Gaussian excitation is applied at node 10, shown in Figure 3.1(b). The signal is obtained by generating a Gaussian distributed vector and passing it through a low-pass digital filter. The filter was designed such that higher modes above 100 Hz will not contribute much to the response.

Acceleration response in the Z-direction was recorded with a sampling interval of 0.0019 seconds. Sensor locations were defined at the nodes of two longitudinal members labeled “spar 1” and “spar 2” in Figure 3.1(b). Hence, 5 sensors were considered on each spar dividing the corresponding spar into 5 segments marked 1 through 5 in Figure 3.1(b). Figure 3.3 illustrates the PSD of obtained excitation signal and the corresponding response in the Z-direction.

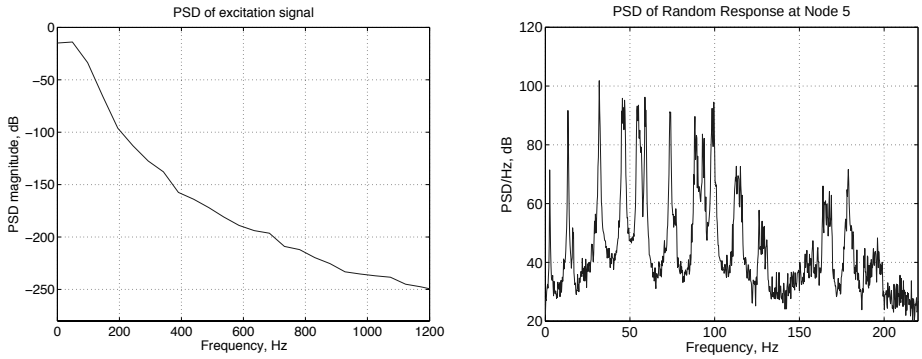

(a) PSD of the excitation signal passed through the low-pass filter.

(b) PSD of the response at node 5 in the Z-direction.

Figure 3.3: PSD of the band-limited excitation signal and the response of the structure.

3.2 Damage modeling

The damage was assumed to be in the form of the crack in one of the longitudinal members. The behavior of cracked structural members is often nonlinear [86] and can be modeled using bilinear stiffness characteristics [87]. The nonlinear beam behavior in ABAQUS can be implemented by generating a user defined dependency between the bending moment and the curvature. Besides the nonlinear bending behavior, nonlinearities for other loading types such as axial or torsional loading are implemented in a similar manner.

A 3-dimensional model of a cracked structural member was created in ABAQUS to generate nonlinear loading vs. displacement relationships for different types of loading. This detailed model represents a part of the structural member represented by a single beam element being 0.6 m long. The model of the cracked member consists of two identical parts joined together along the cross-sectional interface. Figure 3.4 illustrates these two joined parts. The upper half of the cross-section is free to open and close depending on the applied load, and surfaces undergo contact interaction. Nodes belonging to both parts on surfaces

in the lower half of the cross-section are constrained to undergo identical displacements. This scenario represents a crack that is 50 % deep.

Normal interaction between contacting surfaces in the model was defined to allow arbitrary pressure to be transmitted between them after they come into contact ("hard" contact definition), while both contacting bodies may deform at the contact interface. Interaction in the direction tangential to contact surfaces can be defined in ABAQUS by assigning friction properties such as static and kinematic coefficients of friction. For this study we used "rough" contact definition. It implies that no slip occurs after the contact (equivalent of assigning an infinitely large friction coefficient). This is done under the assumption that in the case of an aluminum structural member surfaces on both sides of the crack will be rough, and numerous asperities will prevent noticeable slippage. Detailed modeling of surface asperities and their interaction during the contact is beyond the scope of this work.

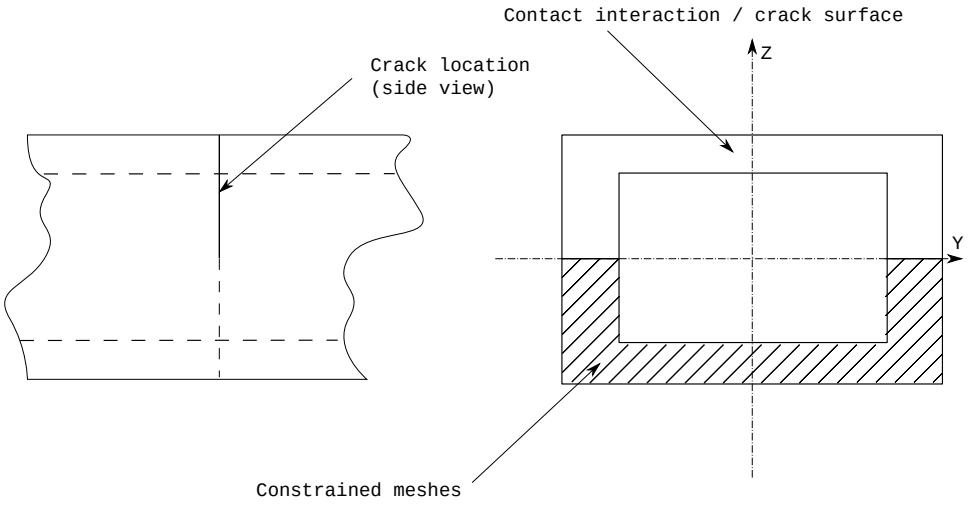

Figure 3.4: Schematic of the cracked section.

Nonlinear loading curves for the damaged member were created for all loading types: axial, torsional, and bending in both planes. For bending loading the nonlinear dependency

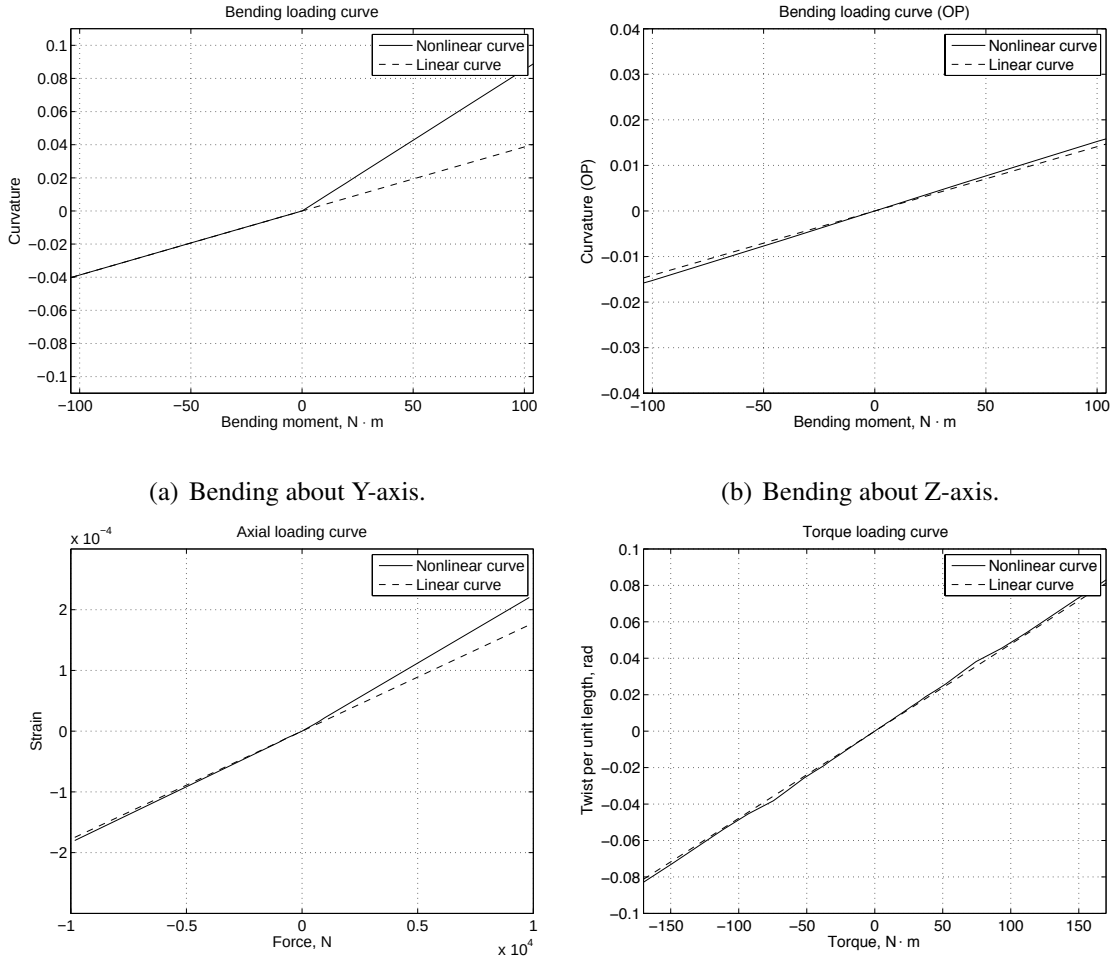

(a) Bending about Y-axis.

(b) Bending about Z-axis.

(c) Axial extension loading.

(d) Torsional loading.

Figure 3.5: Load-deflection curves for the damaged member, crack 50% deep.

is represented by tabulated values of the applied bending moment versus the corresponding curvature of the beam. Similarly, for other loading types tables of strain vs. axial force and twist angle vs. torque were obtained (see Figure 3.5).

For two bending cases, the model represented a beam pinned at both ends. The bending moment was created by applying stresses on the surfaces at the ends of the beam. The

curvature was obtained by using equation (3.1)

$$k = \frac{\frac{d^2y}{dx^2}}{[1 + (\frac{dy}{dx})^2]^{3/2}} \tag{3.1}$$

where derivatives of deflection were calculated using 4^{th} order central differences formulas, which utilize displacements of 5 points uniformly spaced along the neutral axis of the beam.

For the tensile loading case the model represented a cantilever beam with a tensile or compressive stress applied on the surface at the free end. The strain in this case was calculated using corresponding displacement at the free end. For the case of torsional loading, a model with a cantilever beam was used. Twisting moment was created by applying surface tractions of equal magnitudes in opposite directions at the upper and lower halves of the surface at the free end of the beam. The twist angle was calculated by considering in-plane displacements of points on the end surface.

In order to investigate sensitivity of the technique with respect to the severity of the crack, it was decided to consider a case with the crack 25% deep. Load-deflection curves for this case were obtained in the same manner as for the case with a crack 50% deep. The curves representing a crack 25% deep are shown in Figure 3.6. Nonlinearity in this case appears to be noticeably weaker than in the case with the crack 50% deep.

For the case with the crack 50% deep, first the damaged element was assumed to be between nodes 12 and 5; then, the damaged element was assumed to be between the nodes 5 and 8. For the case with the crack 25% deep, only the case with the damaged element between nodes 12 and 5 was considered (see Figure 3.1(b)).

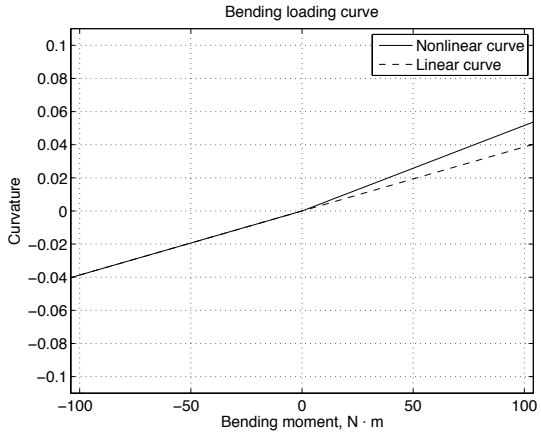

(a) Bending about Y-axis.

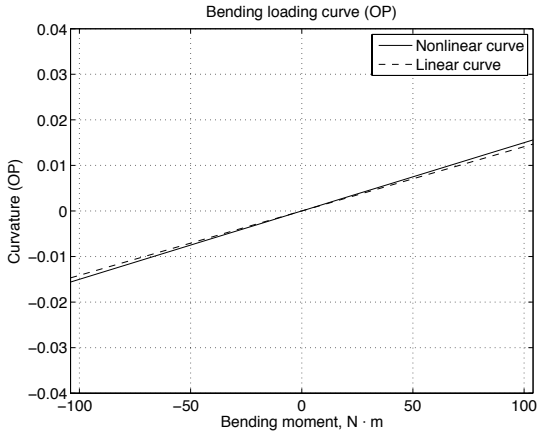

(b) Bending about Z-axis.

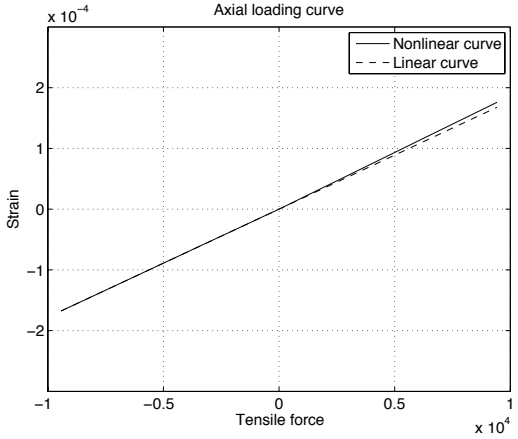

(c) Axial extension loading.

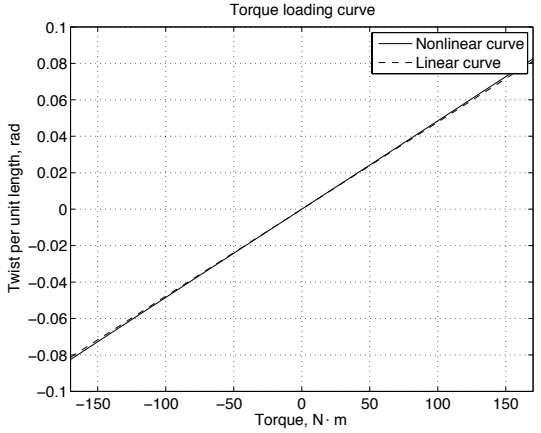

(d) Torsional loading.

Figure 3.6: Load-deflection curves for the damaged member, crack 25% deep.

3.3 Validation

In order to validate the modeling approach utilizing load-deflection curves, another set of curves were obtained that represented an undamaged beam. The purpose of this validation study is not to validate nonlinear load curves, but to ensure that the procedure for obtaining these curves provides reasonably accurate representation of the structural member. In this study we compare displacements predicted by the Abaqus default B32 element with those

predicted by the B32 element utilizing load-deflection curves representing an undamaged structural member.

The study was done using a model of a cantilever beam with 4 different load types as shown in Figure 3.7. The beam is 0.6 m long (equivalent to the length of a single longitudinal segment in the frame model) and was represented by a single element. Loads were applied at the free end of the beam. For each load type the magnitude of the load varied from 0 to 50 units ($N \cdot m$ for moments and N for axial force) with an increment of 10 units. Figure 3.8 contains plots of displacements predicted by the model versus load magnitude. One can observe that the largest relative difference is in the case for the torsional load. This difference is approximately 3.6%, which is acceptable.

Load case	B32 default element	B32 quasi-linear element	Relative Difference, %
Displacement in 2-direction due to bending moment M1	$3.5378 \cdot 10^{-3}$	$3.4809 \cdot 10^{-3}$	1.61
Displacement in 1-direction due to bending moment M2	$1.3028 \cdot 10^{-3}$	$1.2708 \cdot 10^{-3}$	2.46
Angular displacement due to twisting moment T3	$14.949 \cdot 10^{-3}$	$14.414 \cdot 10^{-3}$	3.56
Axial displacement due to tensile force F3	$890.32 \cdot 10^{-9}$	$889.23 \cdot 10^{-9}$	0.12

Table 3.1: Displacements for B32 default element and B32 quasi-linear element, load magnitude 50 units.

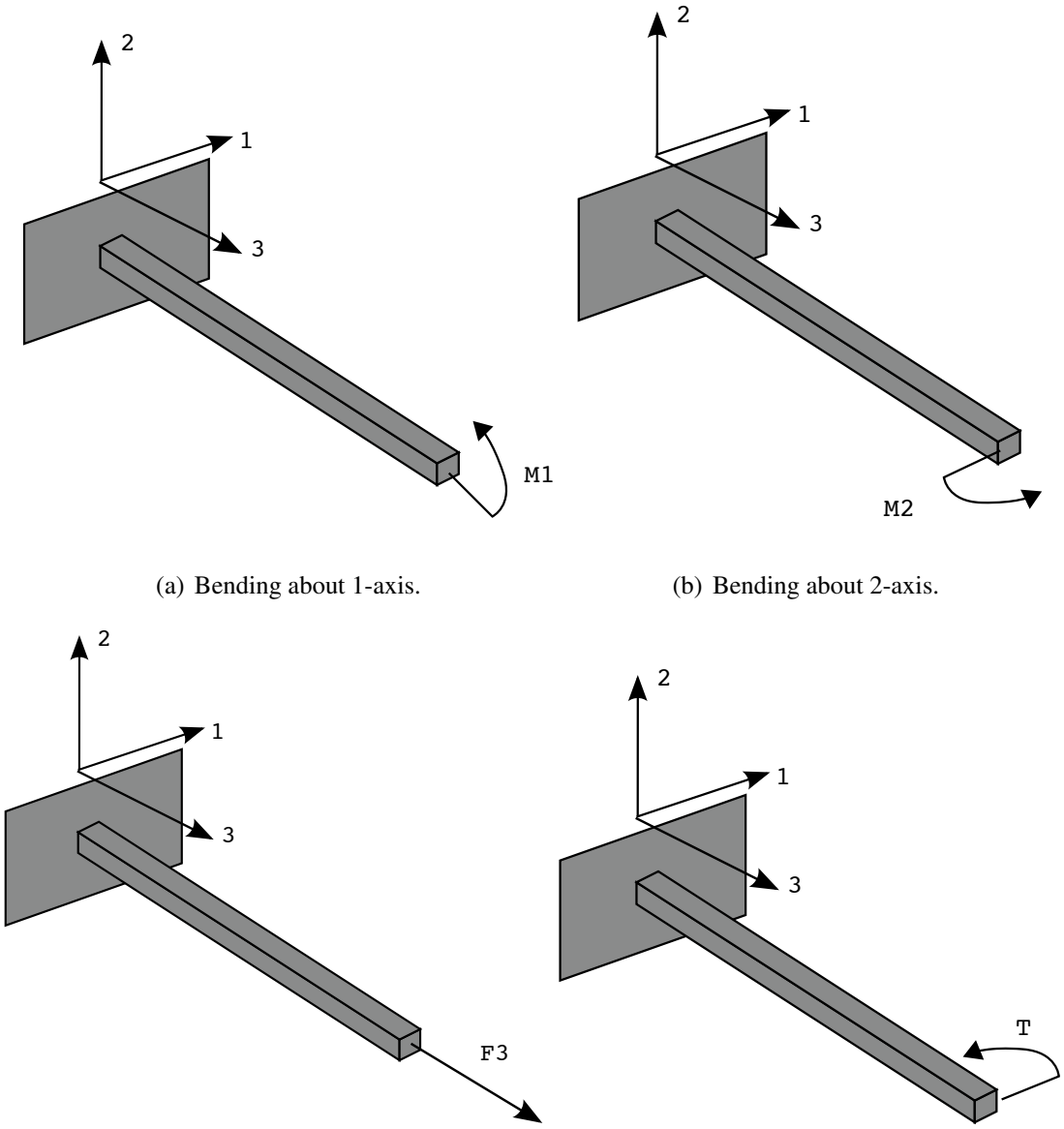

(a) Bending about 1-axis.

(b) Bending about 2-axis.

(c) Axial extension loading.

(d) Torsional loading.

Figure 3.7: Load cases for the validation study.

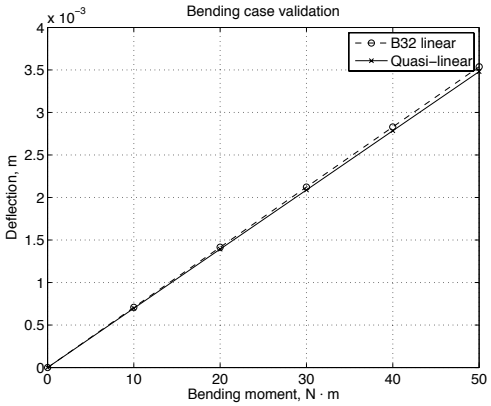

(a) Displacement (m) in 2-direction due to the bending moment M1.

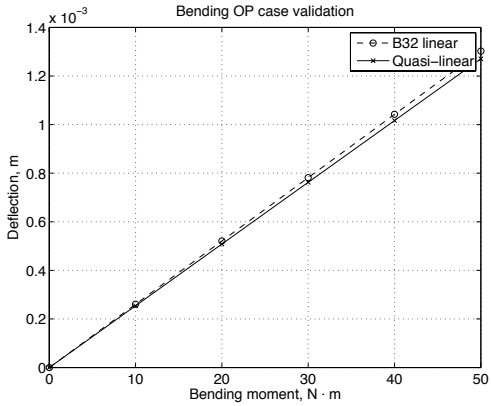

(b) Displacement (m) in 1-direction due to the bending moment M2.

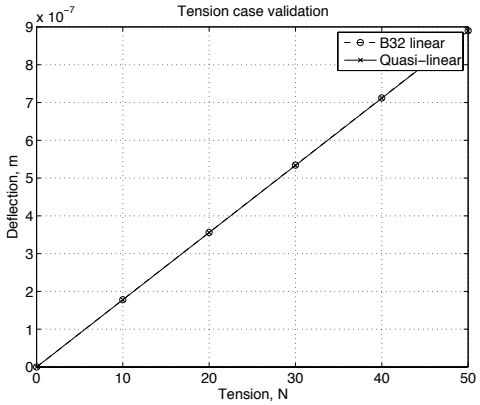

(c) Axial extension (m) in 3-direction due to the tensile force.

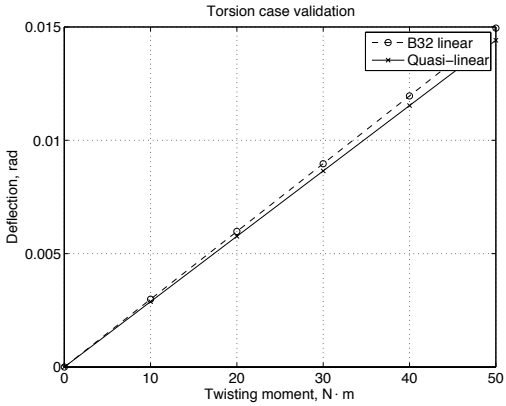

(d) Angular displacement (rad) due to the torque about 3-axis.

Figure 3.8: Displacements obtained in the validation study.

Details of the finite element model of a 3-D frame structure with a damaged structural member were presented. The damage was considered in the form of an opening and closing crack. The procedure for calculation of the load-strain curves for the damaged member was described and validated against the data from a regular B32 element in Abaqus. Application of the method to the simulation data obtained from the model is presented in the next Chapter.

Chapter 4

Application of the Technique to the FEM Simulation Data

4.1 Damage Detection Procedure

The technique that was introduced in Chapter 2 relies on the results of statistical tests to detect and locate nonlinear changes in the structure. In this study, we consider damage to only be in a form of an opening and closing crack, which introduces bilinear stiffness characteristic. Therefore, we consider the change in the means of the Randomdec signatures to identify this damage.

Figure 4.1 shows the outline of the procedure used in this study. Note that it is different from Figure 2.1. First, the measurement data is recorded, zero-meaned, and one calculates the differences between the responses of the neighboring sensors according to DOF connectivity. Those differences represent the dynamic behavior of the segments of the structural members. For example, the difference between responses at nodes 15 and 18

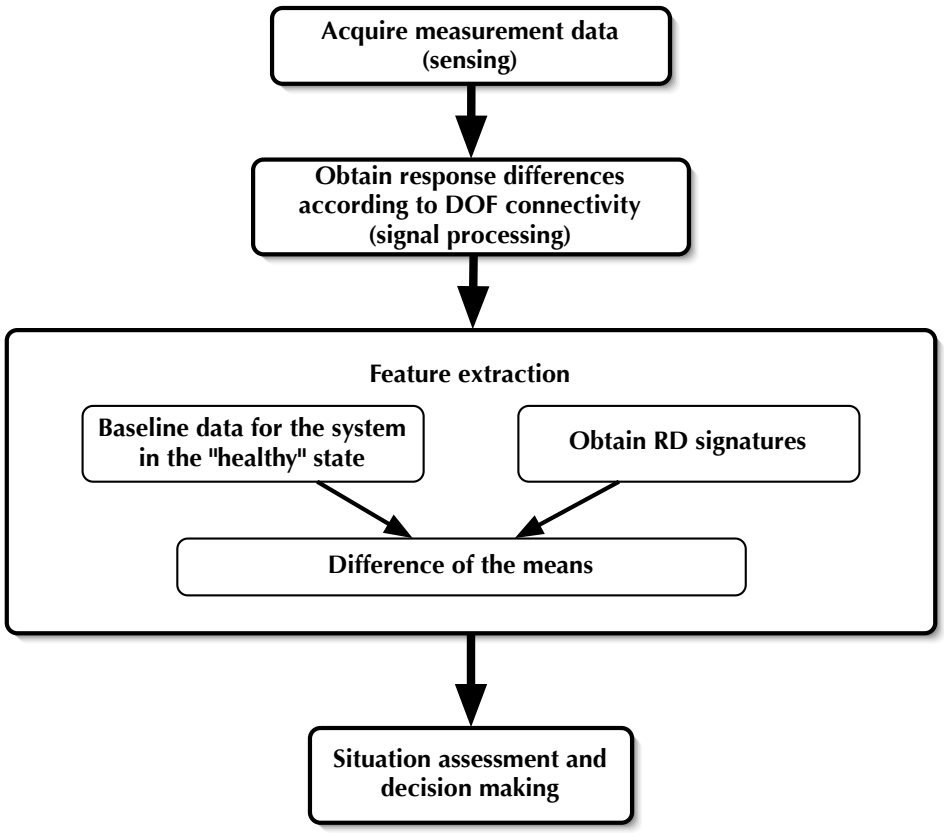

Figure 4.1: Outline of the SHM procedure.

on spar 2 would correspond to segment 2 of spar 2 (see Figure 3.1). Then, RD signatures are calculated from the obtained response differences for both the system in the healthy state (to obtain baseline signatures) and the system in the current state (damaged or not). Absolute value of difference of the means (DMS) is then used as the indicator of damage.

$$DMS_i = |\text{mean}(\hat{D}^i_{XX\text{baseline}}(\tau)) - \text{mean}(\hat{D}^i_{XX\text{current}}(\tau))| \tag{4.1}$$

In practice, one can only record a limited length time history of random response of the system and the signatures calculated from the system in the healthy state will differ slightly from each other due to randomness of excitation. To increase reliability of detection, the

baseline RD signatures are calculated by averaging RD signatures obtained from several realizations of random response. Figure 4.2(a) illustrates the process for calculation of baseline signatures and Figure 4.2(b) describes the feature extraction step of the procedure. In this work, we utilized 20 random response realizations from the system in the healthy state (each 30 seconds long) and 5 realizations for each case of damage.

4.2 Results and Discussion

4.2.1 Cases with crack 50% deep

First, the damaged element was in segment 4 (between nodes 12 and 5) on spar 2; then the damaged element was in segment 5 (between nodes 5 and 8) on spar 2 (see Figure 3.1(b)). In both cases the triggering level for obtaining RD signatures was set for 1.5 of the standard deviation of the response. We applied the technique to the signatures of 2.5 and 3.5 seconds long. In addition to cases with noiseless data, cases were run using response data containing 10% Gaussian noise with 5% bias. "10% noise" implies that the ratio of the standard deviation of noise to the that of the original signal is 0.1; and "5% bias" implies that the bias in the noise added to the data is approximately 5% of standard deviation of the original signal. The amount of bias did not vary with time.

Figures 4.3 and 4.4 contains damage detection results for the case with damage at segment 4 of spar 2. Black bars indicate the absolute difference of the means for the data obtained from the structure with a damaged element. RD signatures for the system in the healthy state also differ from the baseline RD signature and the average results from

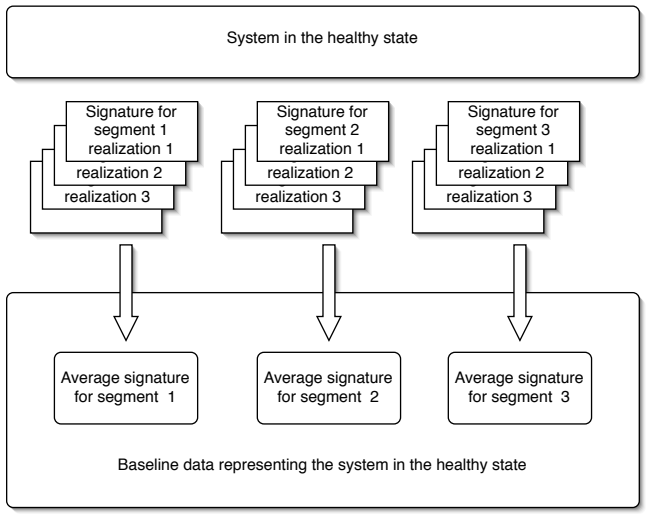

(a) Calculation of baseline signatures by averaging from several realizations.

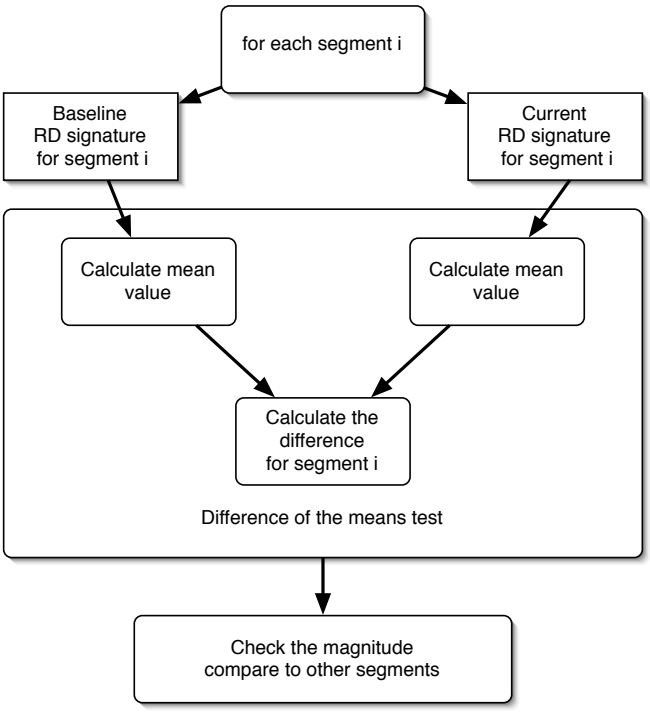

(b) Feature extraction process.

Figure 4.2: Data processing steps in the proposed SHM procedure.

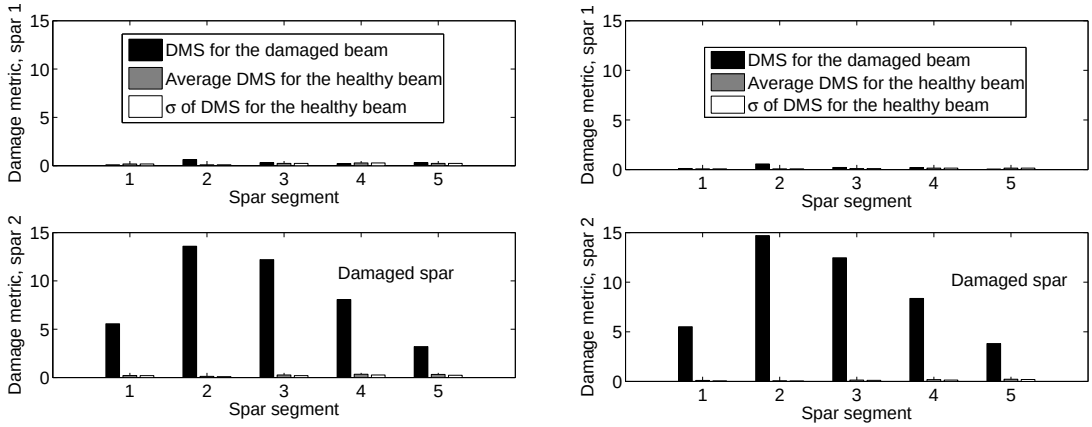

(a) No noise, signature length 2.5 s. (b) No noise, signature length 3.5 s.

Figure 4.3: Diagnosis results for case 1: damage in segment 4 of spar 2, noiseless data.

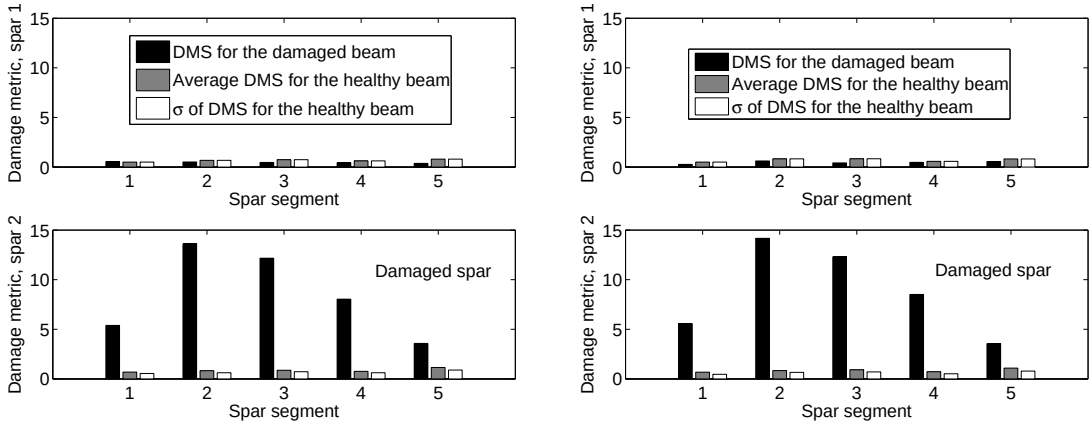

(a) 10% noise with 5% bias, signature length 2.5 s. (b) 10% noise with 5% bias, signature length 3.5 s.

Figure 4.4: Diagnosis results for case 1: damage in segment 4 of spar 2, 10% noise with 5% bias.

equation (4.1) for the signatures of the healthy system are represented by gray bars. The standard deviation of the DMS values calculated from signatures representing the system in the healthy state is represented by white bars.

From results shown in Figure 4.3 one can observe that for the case without noise, significant differences are found for all segments of spar 2 when signatures 2.5 seconds long were used. Also, when signatures 3.5 seconds long were used, significant differences

are found in all segments of spar 2. Although the test did not allow pinpointing of the exact location of the damaged element, it indicated significant change in the vicinity of the damaged element. Diagnostics for spar 1 indicated differences that are comparable to those from the system in healthy state, thus one can conclude that this spar is not damaged.

For the cases with noise added to the measurement data, the average differences calculated for the system in the healthy state are noticeably larger than those from noiseless data, which can reduce reliability of detection. From results in the cases with 10% noise and signatures 2.5 seconds long, one can conclude that significant change is again in all segments of spar 2. Similarly, for the case with signatures 3.5 seconds long, significant change is observed in all segments of spar 2. As in the case with no noise added to the measurements, values calculated for spar 1 are comparable to those from the system in the baseline state. From results shown in Figures 4.3 and 4.4 it is difficult to draw conclusions about the effect of the length of the RD signatures on damage detection.

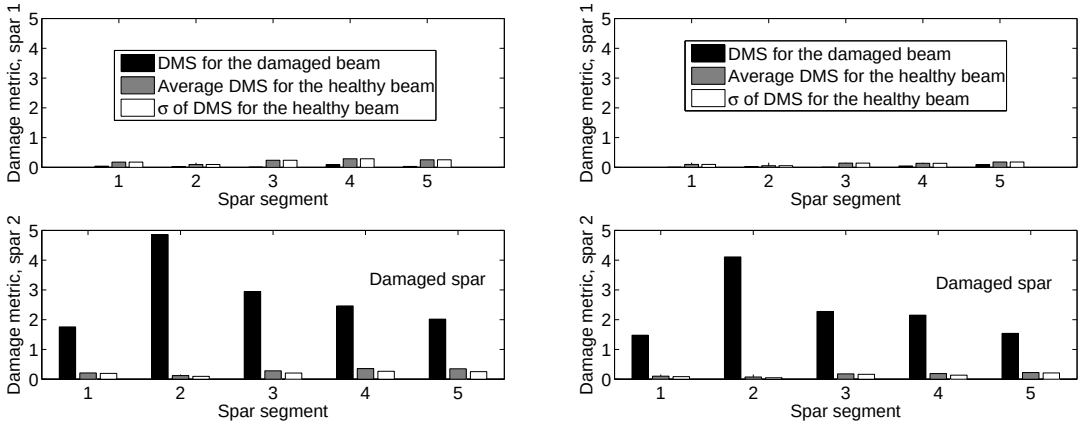

(a) No noise, signature length 2.5 s. (b) No noise, signature length 3.5 s.

Figure 4.5: Diagnosis results for case 2: damage in segment 5 of spar 2, noiseless data.

Figures 4.5 and 4.6 illustrate results for the case when damage is located in segment 5 of spar 2. Results obtained for case with noiseless data suggest that significant changes

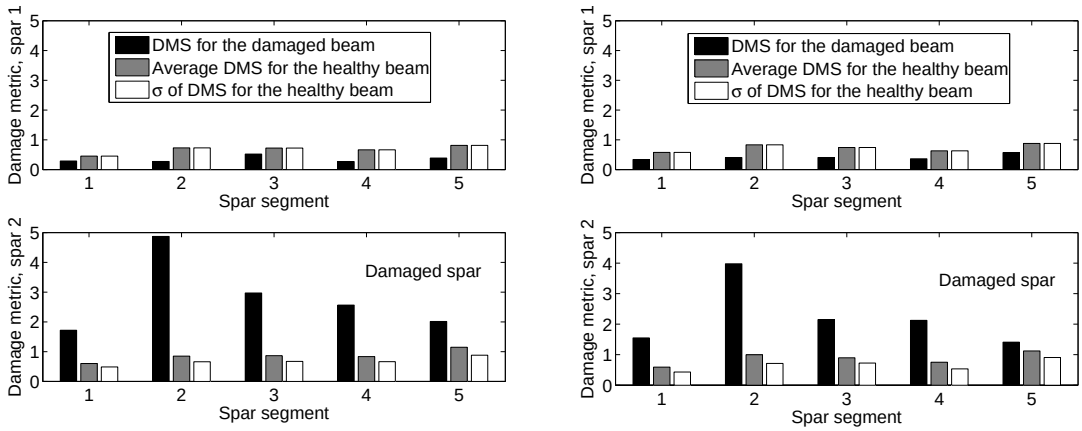

(a) 10% noise with 5% bias, signature length 2.5 s. (b) 10% noise with 5% bias, signature length 3.5 s.

Figure 4.6: Diagnosis results for case 2: damage in segment 5 of spar 2, 10% noise with 5% bias.

occurred in all segments of spar 2 with the largest values obtained for segments 2, 3, and 4.

For the cases when 10% noise was added, diagnostic results indicate the presence of damage in segments 1, 2, 3, and 4 of spar 2 (in both cases with signatures 2.5 and 3.5 seconds long). Although the technique did not indicate the exact location of damaged segment, it was able to indicate onset of nonlinearity in the vicinity of the actual damage. Also, it was observed that noise added to the measurement data blurs the changes in the response due to damage.

4.2.2 Cases with the crack 25% deep

Figure 4.7 contains results after applying the technique to noiseless data from a model with quarter cross-section crack in segment 4 of spar 2 (see Figure 3.1). The results indicate that significant changes are detected in spar 2, whereas spar 1 remains healthy. Most significant changes are indicated in segments 2, 3, and 5, but not segment 4. As in the previous cases,

the test did not indicate the precise location of the cracked member, but at least indicated the damaged spar.

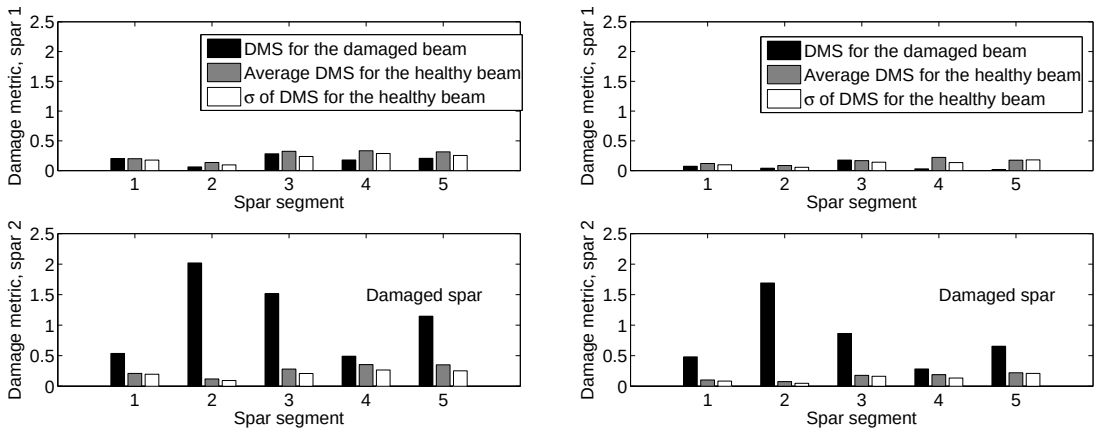

(a) No noise, signature length 2.5 s. (b) No noise, signature length 3.5 s.

Figure 4.7: Diagnosis results for the case with the crack 25% deep: damage in segment 4 of spar 2, noiseless data.

Figure 4.8 contains results after applying the technique to acceleration data with 10% noise with 5% bias. The results indicate that there are no statistically significant changes. For both spars the magnitude of the damage metric is within 2 standard deviations of its mean value for the system in the healthy state. Figure 4.9 contains results for the same case of damage, but only 5% noise is added. Significant changes are detected in segment 2 of spar 2 allowing detection of the damaged spar.

In order to compare the results for the crack 25% and 50% of cross-section deep, one needs to examine Figures 4.3 and 4.7. For the signatures 2.5 seconds long, the maximum magnitude of the damage metric occurs in segment 3 of spar 2 for the crack 50% deep, while for the crack 25% deep it occurs in segment 2 of spar 2. For the crack 50% deep the maximum magnitude of the damage metric is ≈ 4.6, while for the crack 25% deep it is ≈ 2.0 (2.3 times smaller). For signatures 3.5 seconds long, the maximum magnitude of the

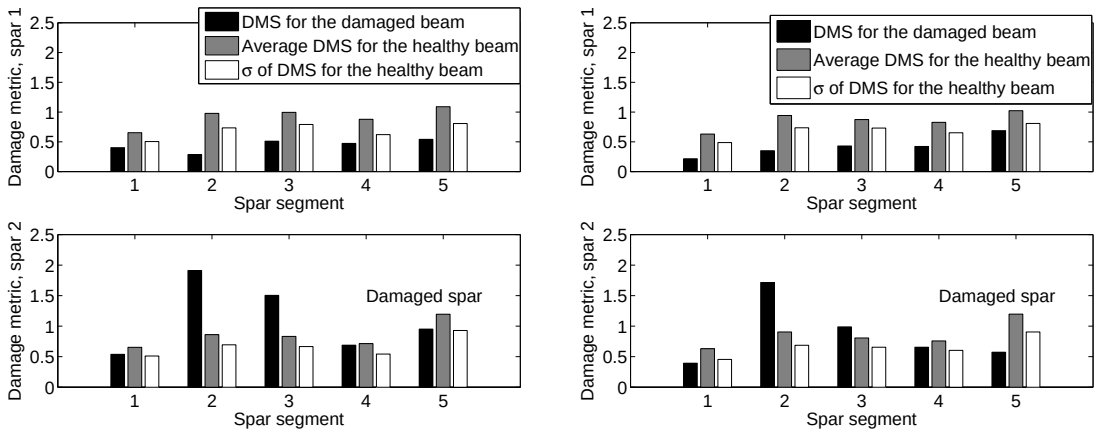

(a) Noisy data, signature length 2.5 s. (b) Noisy data, signature length 3.5 s.

Figure 4.8: Diagnosis results for the case with the crack 25% deep: damage in segment 4 of spar 2, data with 10% noise.

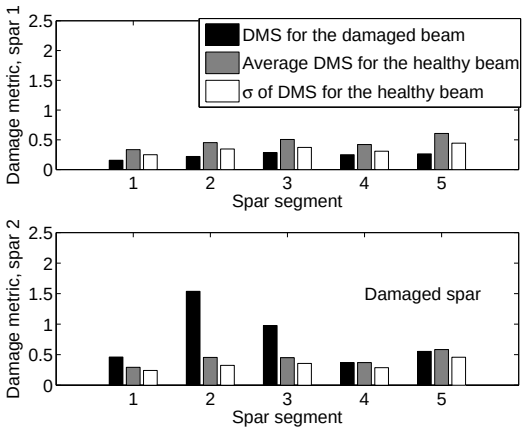

Figure 4.9: Diagnosis results for the case with the crack 25% deep: damage in segment 4 of spar 2, data with 5% noise.

damage metric is ≈ 2.9 for a crack 50% deep, and ≈ 1.7 for a crack 25% deep (1.7 times smaller). Thus, the magnitude of the damage metric increases with increasing crack depth. Also, shorter signatures produce higher magnitudes of the damage metric.

4.2.3 Results obtained under low excitation

Virtually all real world systems are nonlinear to some degree, however observation of nonlinear features in their responses often depends on excitation levels. At lower excitation levels nonlinearities are not as easily detected. This study investigates the capability of the method using simulated measurement data from a much lower excitation level. Excitation level was reduced from $\sigma_F = 100$ N to 10 N. The damage was considered to be a crack 50% of cross-section deep located in segment 4 of spar 2.

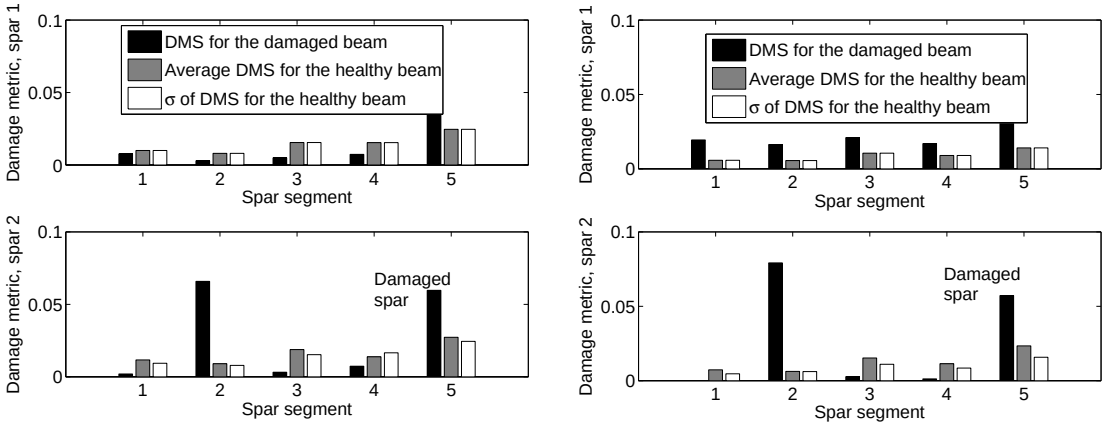

(a) No noise, signature length 2.5 s. (b) No noise, signature length 3.5 s.

Figure 4.10: Diagnosis results for the case with low excitation: damage in segment 4 of spar 2, noiseless data.

Figure 4.10 illustrates results for the case with noiseless data. The results indicate that there is a very significant change in the damage metric for segment 2 of spar 2, but the changes in spar 1 are not nearly as significant. Figure 4.11 presents the results for the case with 10% noise with 5% bias added. From these results one can conclude that changes in the damage metric are comparable to those for the system in the healthy state. Presence of large amount of noise in the measurements did not allow detection of damage. Figure 4.12 illustrates results obtained with the noise reduced to 5% instead of 10%. In this case

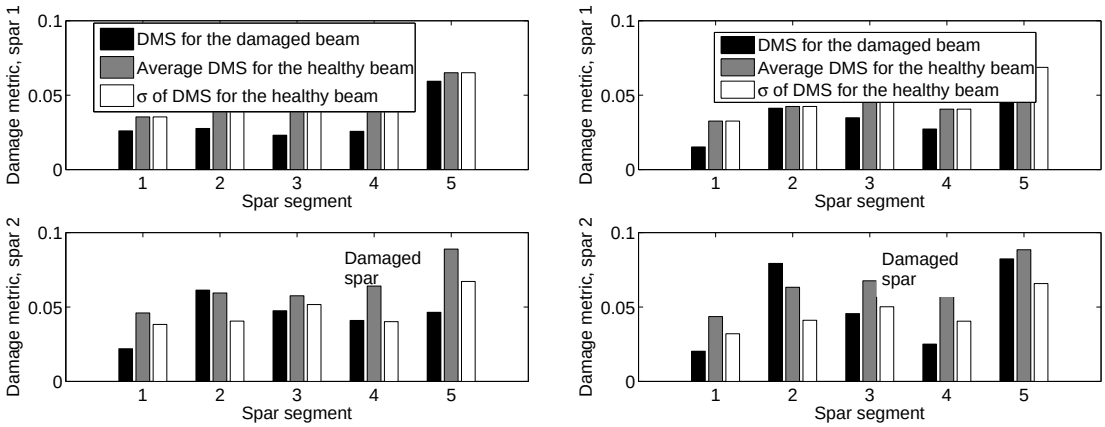

(a) 10% noise with 5% bias, signature length 2.5 s. (b) 10% noise with 5% bias, signature length 3.5 s.

Figure 4.11: Diagnosis results for the case with low excitation: damage in segment 4 of spar 2, 10% noise with 5% bias.

a significant change in the damage metric is indicated for segment 2 of spar 2. Therefore, for instances when excitation levels are low or cracks are relatively small reliability of detection will depend on the amount of noise present in the measurements.

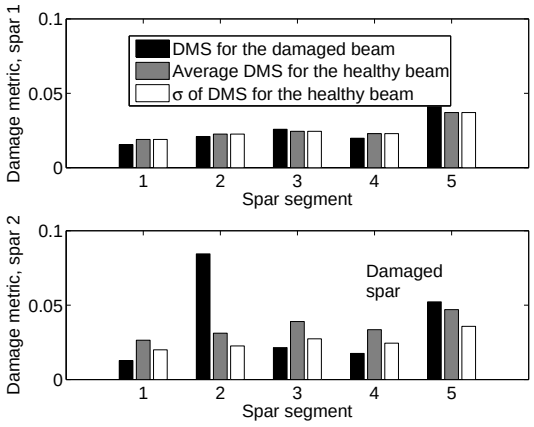

Figure 4.12: Diagnosis results for the case with low excitation: damage in segment 4 of spar 2, data with 5% noise, signature length 3.5 s.

An additional investigation was performed to test susceptibility of the the method to produce false alarms when excitation level of the baseline data was different from that of the current data. In all cases noiseless data from undamaged system deep was used. First,

baseline data was considered from simulations using low excitation levels ($\sigma_F = 10$ N). The corresponding test data was taken from the previous study with $\sigma_F = 100$ N. Then, data from simulations with $\sigma_F = 100$ N was considered for baseline signatures, and the test data came from simulations with $\sigma_F = 10$ N.

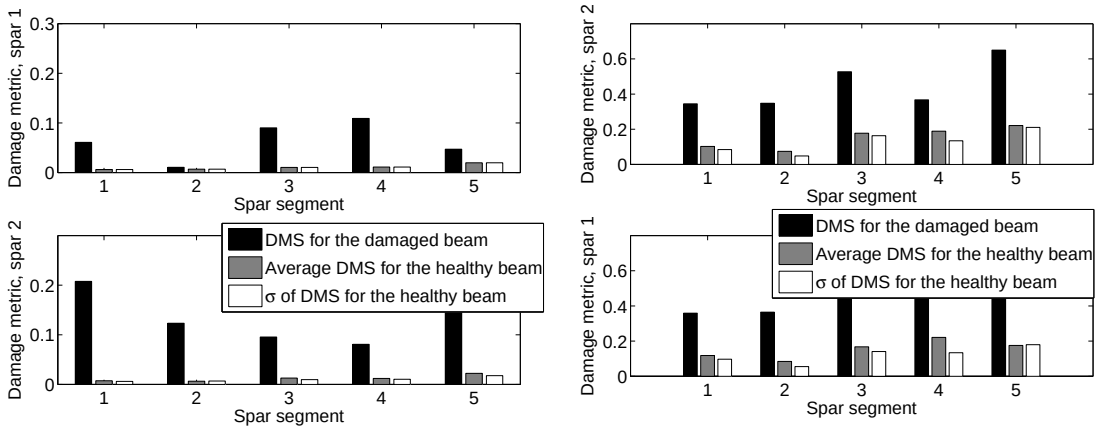

(a) Results with the baseline data from low excitation level.

(b) Results with the baseline data from high excitation level.

Figure 4.13: Diagnosis results for the cases with baseline and test data obtained from different excitation levels. All data came from the system in the healthy state.

From Figure 4.13 one can observe that in both cases the method resulted in significant changes in the damage metric for most segments of both spars, although test date from the system in the healthy state was used. This indicates that the method is susceptible to false alarms when excitation levels of the baseline data and the test data are significantly different (in this case the difference is actually rather large, $\sigma_F^{high}/\sigma_F^{low} = 10$). In practice, for structures excited by ambient forces it is reasonable to assume variation of excitation levels in time. For example, some days may have stronger winds than others. To reduce the likelihood of false alarms due to excitation levels, both baseline and test data should be collected across a wide range of excitation conditions.

4.2.4 Effects of randomdec signature parameters on damage detection

It is of interest to study the reliability of damage detection with respect to the length of the randomdec signatures and the triggering level that was used to calculate them. Previous studies were done using a single triggering level ($1.5\sigma_{\ddot{x}}$) and only two different signature lengths were considered - 2.5 and 3.5 seconds. The mean value of the signature fluctuates depending on its time length. Shorter randomdec signatures may not contain a large enough number of time samples, thus its mean value can vary significantly. This can potentially cause false alarms, which is not desirable. Also, it is not clear how the triggering level affects the mean values of the signatures and damage detection.

In this study we considered 5 triggering levels in the range $[0, 2]\sigma_{\ddot{x}}$ with an increment of $0.5\sigma_{\ddot{x}}$. For each triggering level, randomdec signatures of five time lengths were considered: 0.5, 1.5, 2.5, 3.5, and 4.5 seconds. Hence, a total of 25 cases were considered. Noiseless acceleration data for the case with the crack 50% deep in segment 4 of spar 2 was used.

Figure 4.14 illustrates absolute values of the DMS criterion obtained in this study. Plots in the left column represent the values of the DMS criterion obtained for spar 1. The right column represents spar 2. Absolute values of the DMS criterion obtained for shorter signatures (0.5, 1.0 seconds long) for most segments are larger than these obtained from longer signatures. Also, for cases with higher triggering level, absolute values of the DMS criterion tend to increase.

Figure 4.15 shows the relative magnitude of the DMS criterion with respect to the

standard deviation of the damage criterion for the system in the healthy state. For the signatures 0.5 seconds long, there is a significant change in the DMS criterion for segment 2 of spar 1, which represents a false detection. Note that for longer RD signatures and higher triggering levels the relative magnitude of the damage metric is close to 1 for the undamaged spar, but reaches the values of that are almost two orders of magnitude higher for most segments of spar 2. This results in the conclusion that reliability of detection increases with the signature length and higher triggering levels.

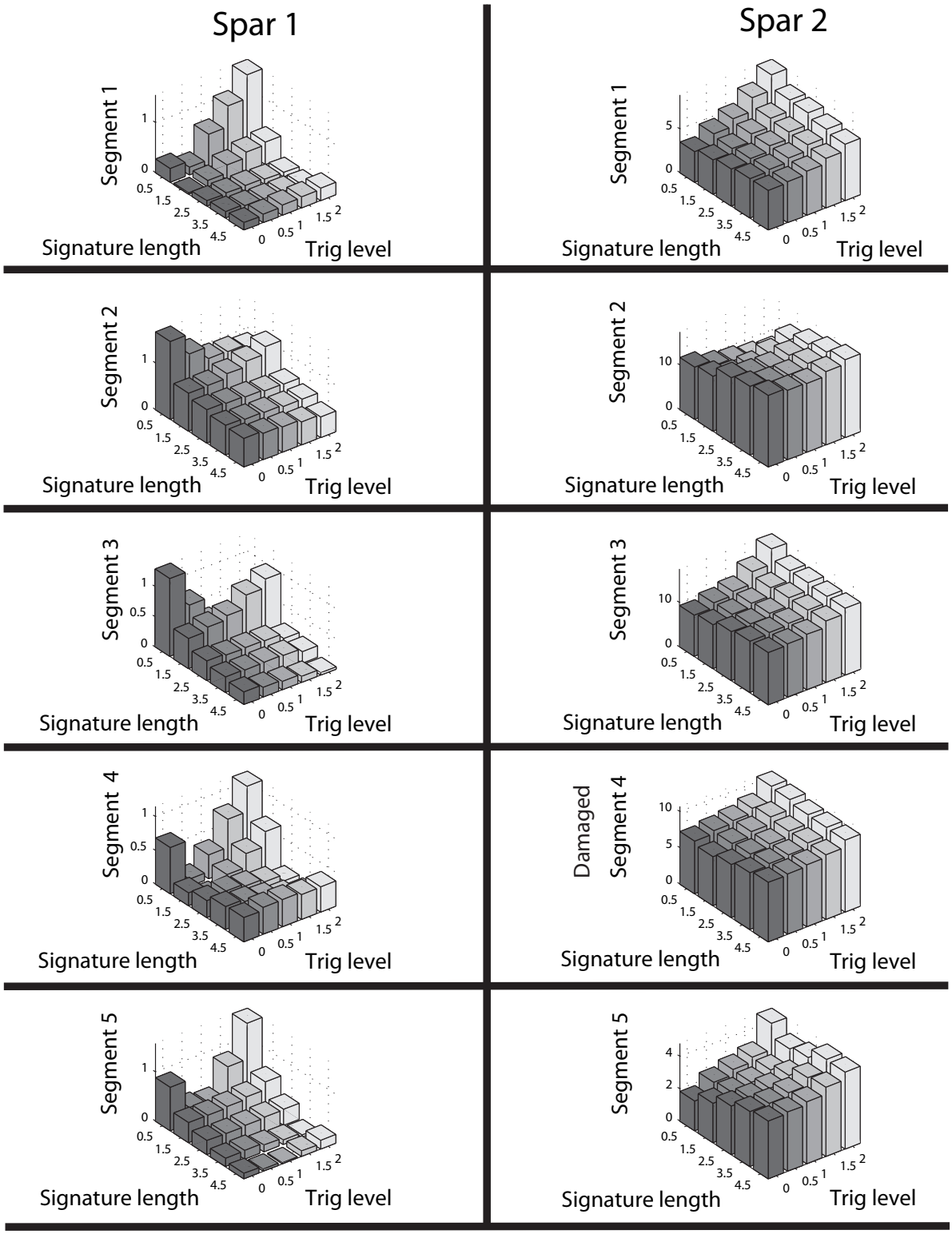

Figure 4.14: Absolute values of the DMS criterion obtained across the range of triggering levels and signature lengths.

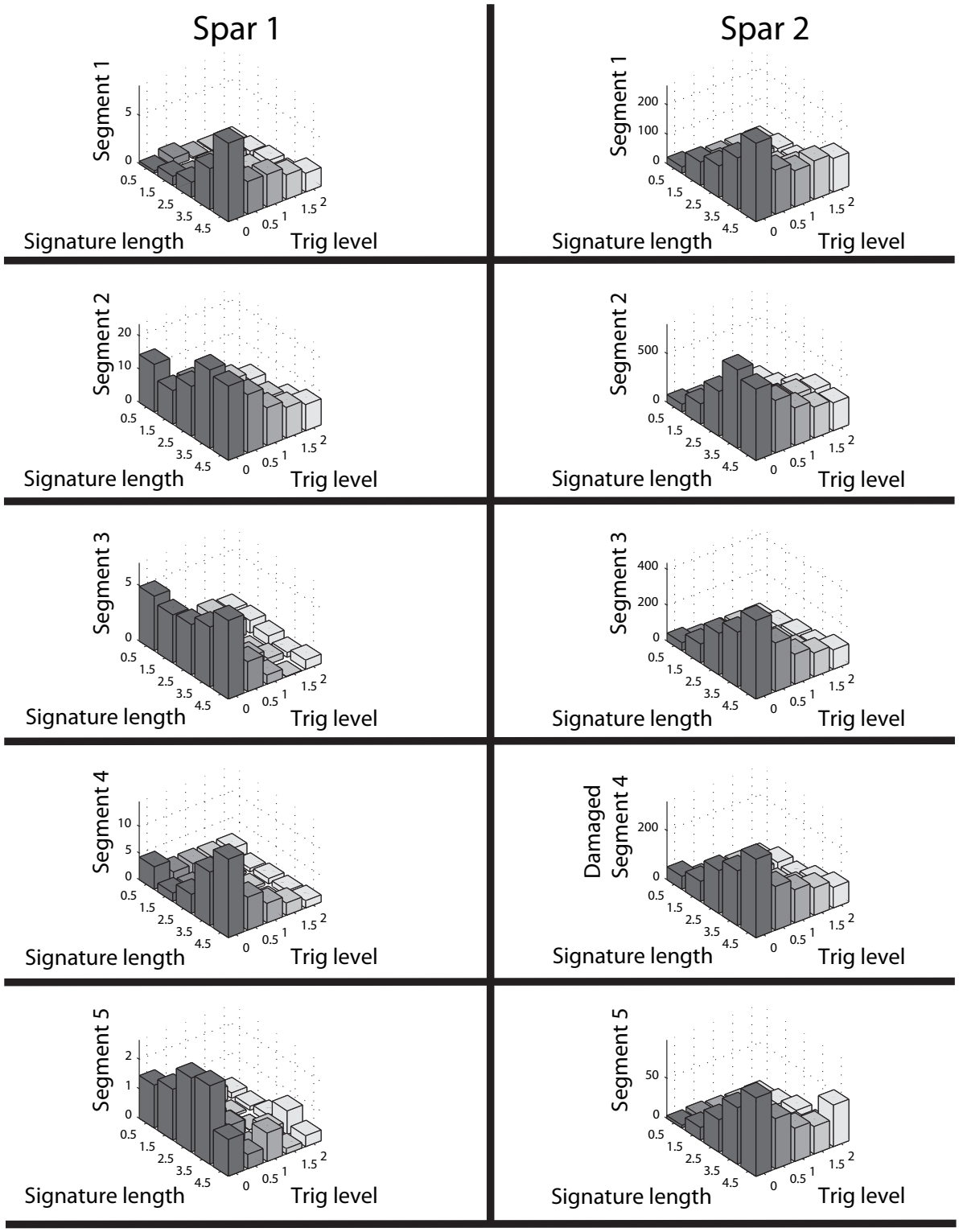

Figure 4.15: Relative values of the DMS criterion obtained across the range of triggering levels and signature lengths.

Chapter 5

Experimental Validation

5.1 Experiment setup

The experiment is designed to validate the ability of the technique to detect a breathing crack in a cantilever beam. The beam is made of 2024-T351 aluminum. Figure 5.1 shows the schematic of the experiment. The beam is 30 inches long with solid rectangular $1 \times 1/2$ in. cross-section. The specimen is mounted on the Unholtz-Dickie S032 shaker using a clamp machined out of 7075 aluminum. High rigidity and low weight are desired characteristics for vibration fixtures because they allow to minimize the dynamic effects of the fixture on the test results. Heavy fixtures and specimen may significantly limit shaker performance. The clamp was designed to provide durability, high rigidity, and reduced weight.

Acceleration measurements were obtained using five PCB 352C22 miniature accelerometers placed along the beam. Figure 5.1(b) illustrates sensor locations. Data were recorded using LabView BNC-2120 adapter with PCI-6024E DAQ card with a sampling rate set at 10100 Hz. This sampling rate was chosen because the DAQ card does not have anti-

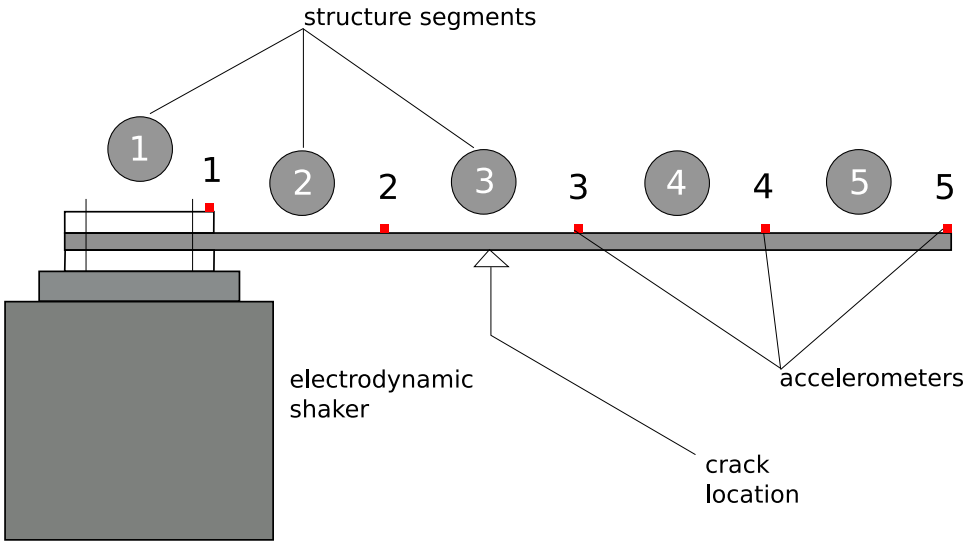

(a) Beam segments.

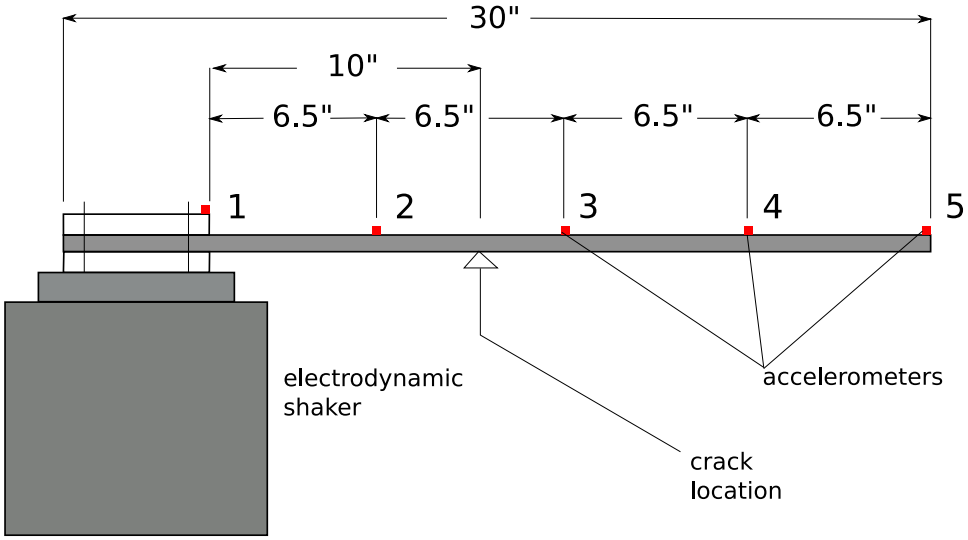

(b) Beam geometry.

Figure 5.1: Cantilever beam experiment.

aliasing filters and, as a result, it is necessary to employ very high sampling rate. Agilent 33120A function generator provided white noise excitation signal. The signal was passed to the shaker amplifier through the Ithaca low-pass filter filter with a corner frequency of 1000 Hz. This was done to avoid excitation of higher modes and internal resonances in the shaker and the clamp.

Figure 5.2(a) shows the power spectrum density of the signal output from the Ithaca filter that is inputted into the shaker amplifier. Figure 5.2(b) illustrates the power spectrum density of acceleration measured on the clamp. One can notice the shaker armature resonance at around 3000 Hz.

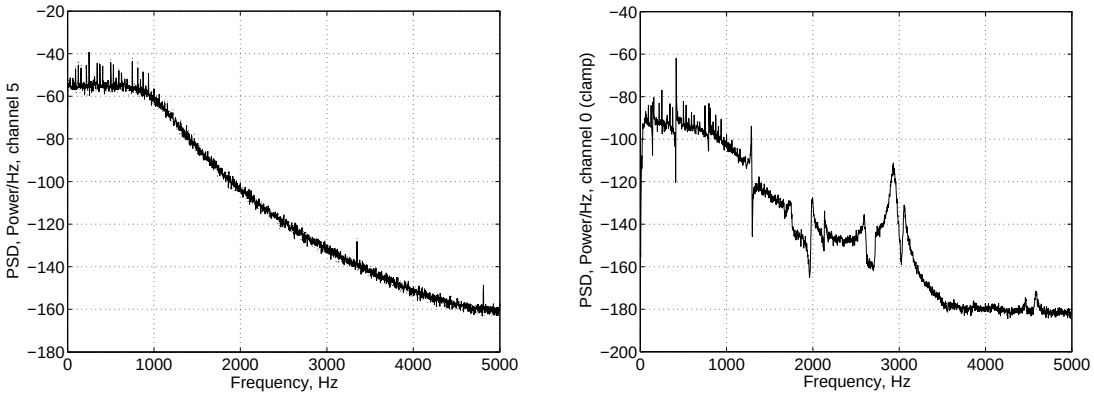

(a) PSD of the signal supplied to the shaker amplifier. (b) PSD of acceleration measured on the clamp.

Figure 5.2: PSD of excitation signal.

The damaged specimen was produced by growing a crack from a very sharp notch made on the top surface of the beam at the axial location that corresponds to segment 3 in Figure 5.1(a). A similar size notch was produced in the baseline specimen, but with a dull cutter to avoid creating a sharp stress concentrator. Sonntag SF-1-U fatigue testing machine with a bending fixture was used to grow a crack in the damaged specimen (Figure 5.3). The crack produced in the beam is located between two black lines (Figure 5.4) with

a penny coin serving as a dimensional reference. Clearly, the crack is very thin and difficult to see with the naked eye on an unpolished surface.

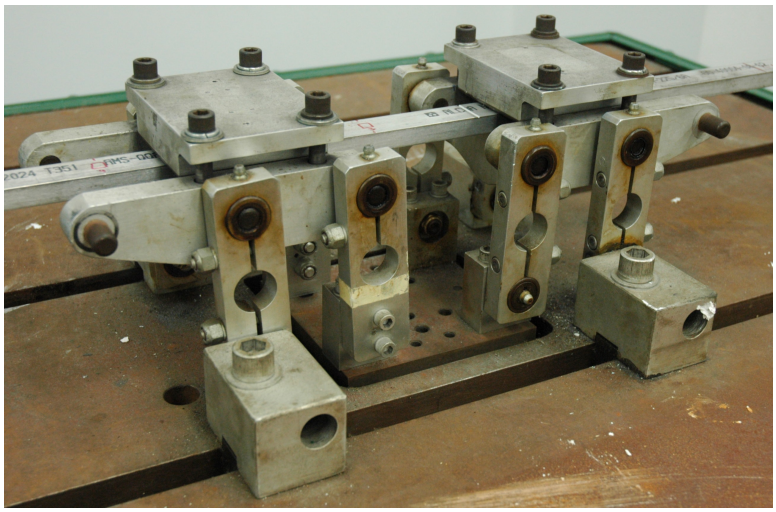

Figure 5.3: Beam specimen mounted in a 4-point bending system.

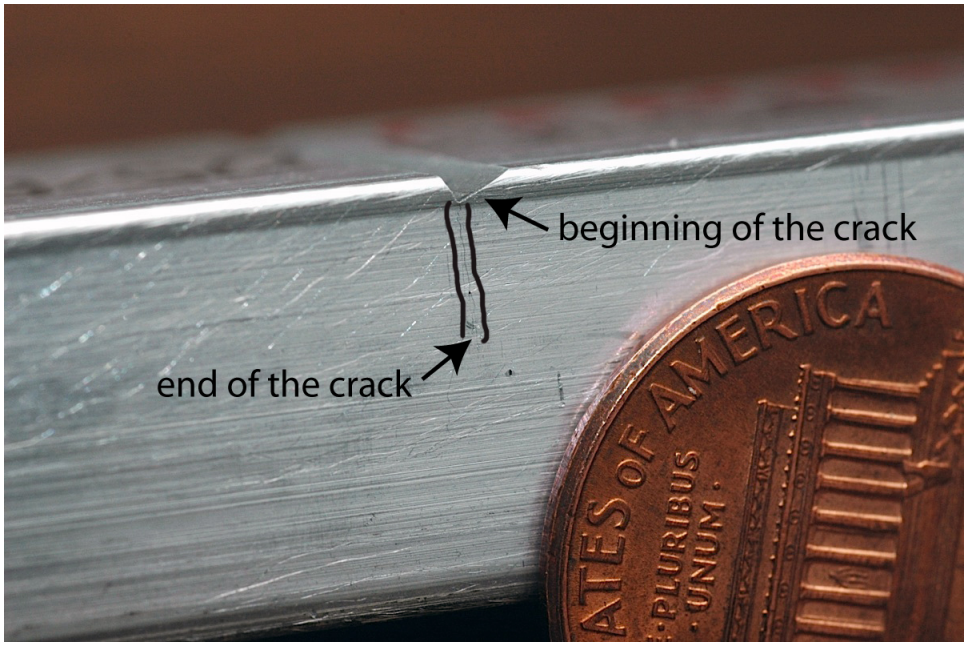

Figure 5.4: Crack in the damaged specimen.

Figure 5.5 shows the plots of the power spectrum density for the healthy and the damaged beams. The resonant frequencies of lower modes are very similar, but a visible difference can be observed for the fifth bending mode at approximately 1200 Hz. Fig-

ures 5.6-5.10 illustrate the changes in the resonant frequencies for the first 5 modes with respect to the excitation levels. Frequency values shown in these figures were obtained by averaging the values obtained from 10 response time histories recorded at each excitation level. Error bars indicate the standard deviation of the resonant frequencies at each excitation level. Relative percent differences were calculated with respect to the resonant frequencies of the healthy beam. One can obsereve that in general the resonant frequencies of the cracked beam are smaller than those of the healthy beam. The difference is more pronounced in higher modes and increases with excitation level.

The average relative difference for the first mode frequency across the range of excitation levels is approximately 0.5%. Also, one can note that the average values for the first mode frequency of the cracked beam are within the standard deviation from the value obtained for the healthy beam. Relative difference in the frequency of the second mode is about 2% and the average values for healthy and cracked beams are further than one standard deviation apart indicating a significant difference. For the 3rd and 5th modes the average relative differences are approximately 1.6% and 2.6% respectively, and in both cases the differences are statistically significant. The 4th mode appears to be the least affected as the average relative difference in the frequency of the healthy and the cracked beams is approximately 0.2%, and the difference becomes statistically significant only at higher excitation levels (1.75g and 2.45g RMS).

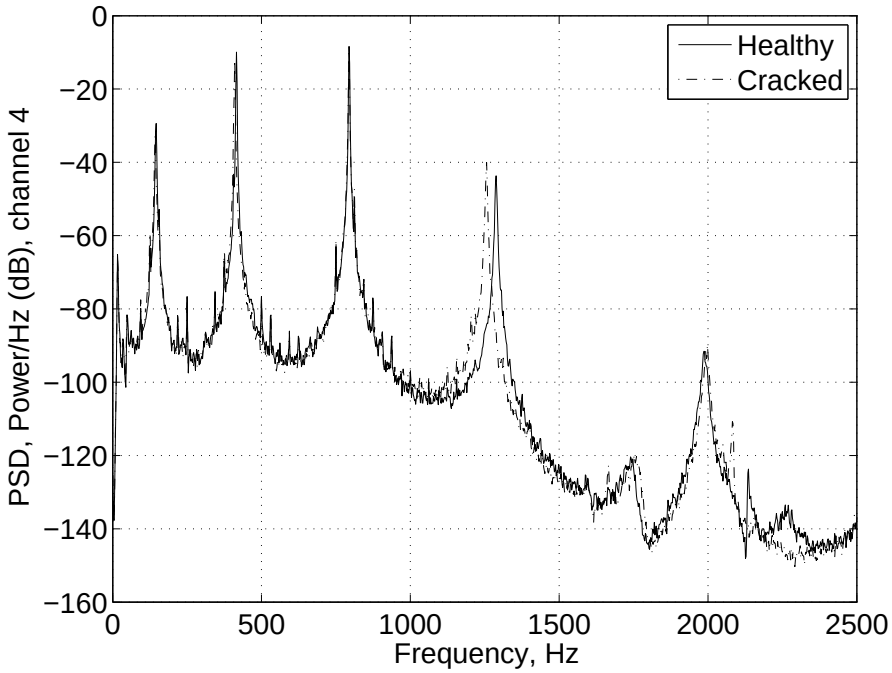

Figure 5.5: PSD of the healthy and damaged beams (1.75g rms).

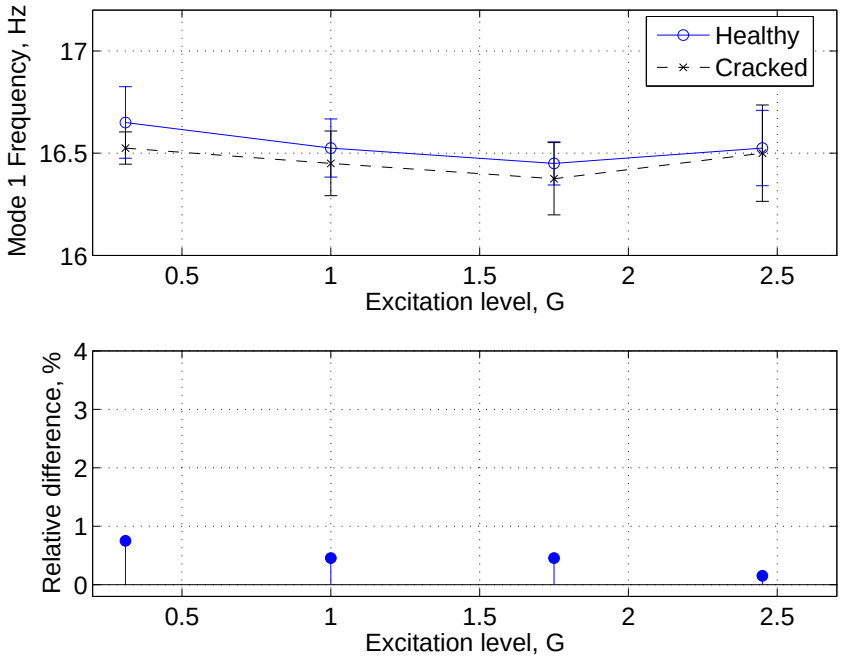

Figure 5.6: First resonant frequency.

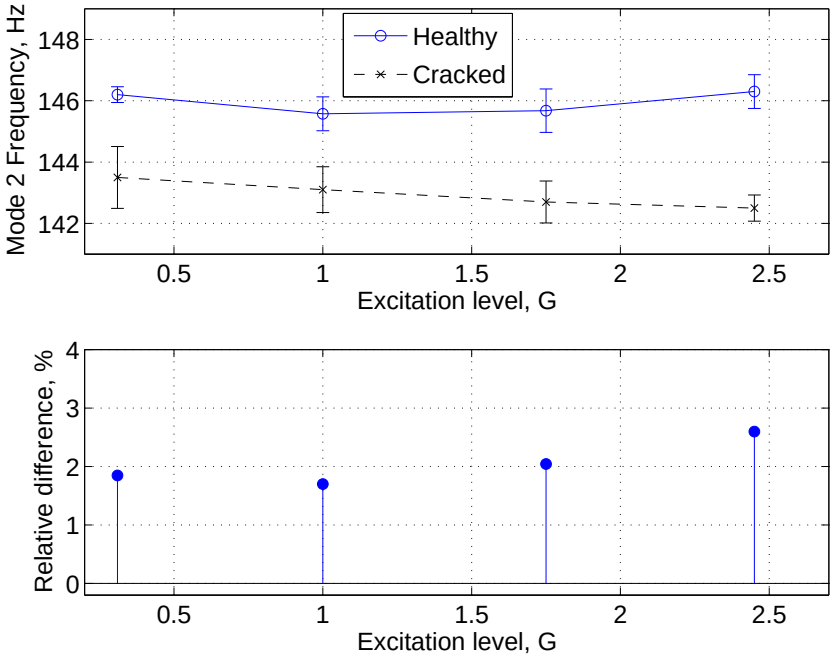

Figure 5.7: Second resonant frequency.

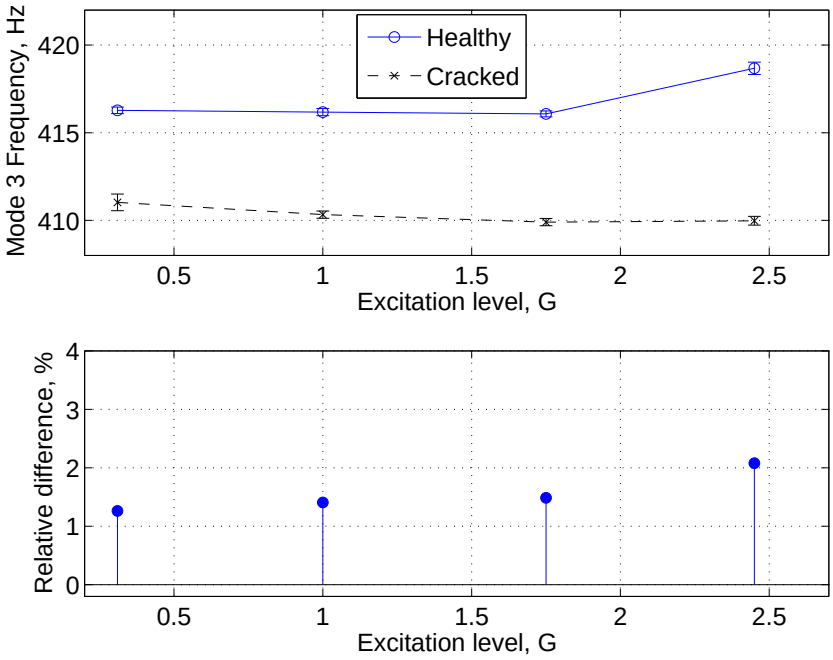

Figure 5.8: Third resonant frequency.

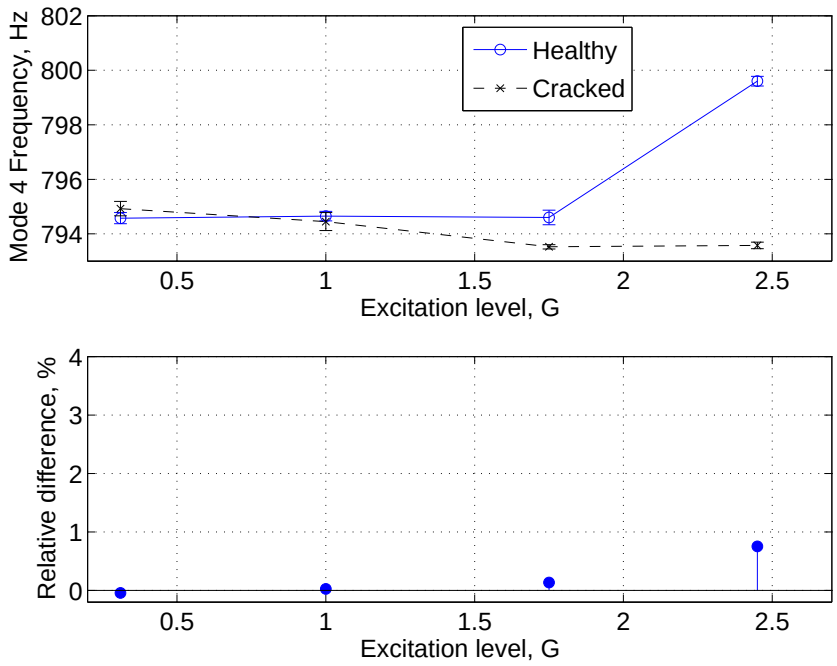

Figure 5.9: Fourth resonant frequency.

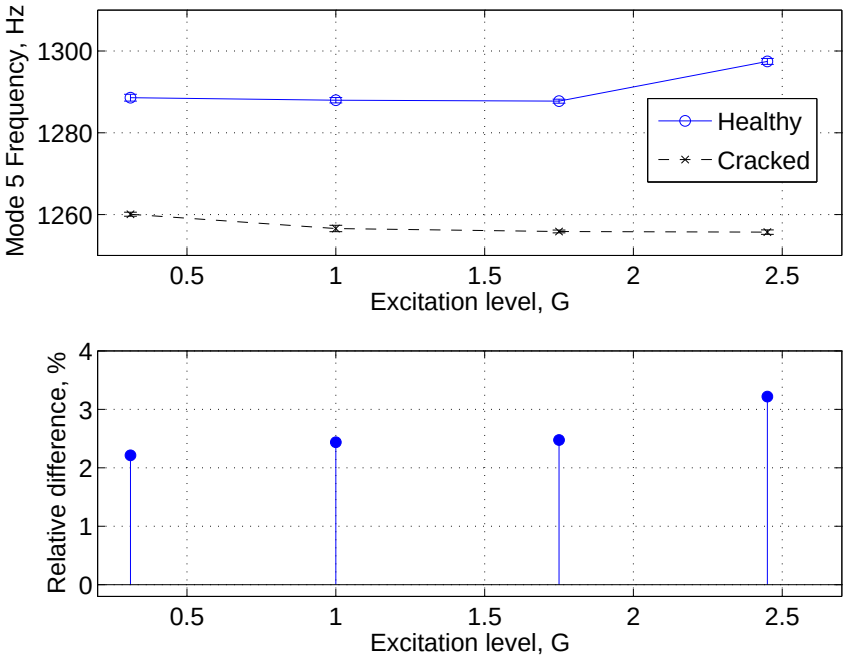

Figure 5.10: Fifth resonant frequency.

5.2 Damage Detection Results

First, the damaged beam was mounted with the notch and the crack facing upwards. In this study, four excitation levels were considered because detection of nonlinearities is expected to be dependent on excitation levels. The lowest excitation level corresponded to ≈ 0.31g RMS at the clamp, and remaining cases corresponded to 1.0g, 1.75g, and 2.45g RMS measured at the clamp. First, the baseline specimen was mounted on the shaker and acceleration data was recorded at all four excitation levels. Then the damaged specimen was mounted and the data was recorded for similar excitation levels. Ten 20-second long acceleration data histories from healthy and damaged specimens were recorded at each excitation level. It must be noted that each 20-second data set was recorded at a random time interval from end of the previous data set, ranging from approximately 1 to 5 minutes.

The damage detection procedure was applied as described in Section 4.1. From results of Chapter 4, it was decided to keep the triggering levels high (1.5σ and 3.0σ of measured response) and use signatures of 2.0 and 2.5 seconds long. Figure 5.11 illustrates 2.5 seconds long signatures for segment 4 of the healthy and damaged beams. Clearly, after approximately 2 seconds, minor variation of the mean value with time is observed.

Figures 5.12-5.15 show the results of applying the damage detection technique to experimental data. Similar to results shown in Chapter 4, the black bars indicate the absolute difference of the means for the data obtained from the damaged beam. Average values of the DMS criterion for the healthy beam are represented by gray bars. The standard deviation of the DMS values calculated from signatures representing the healthy beam is represented by white bars. From experience and engineering judgement, a significant

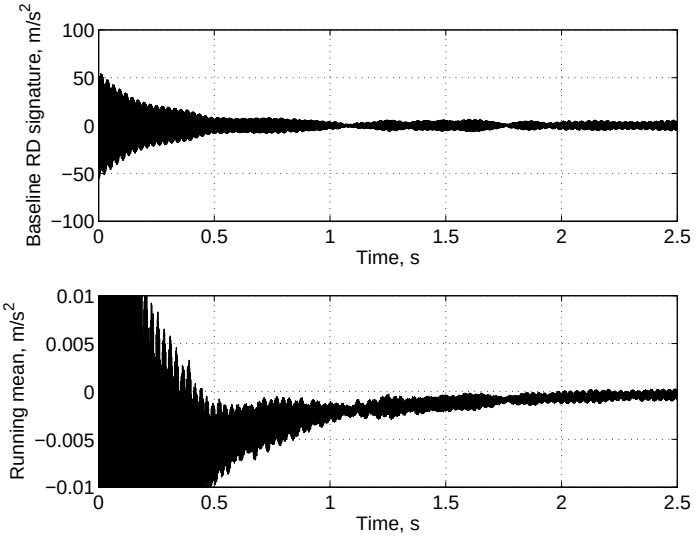

(a) Baseline RD signature and its running mean.

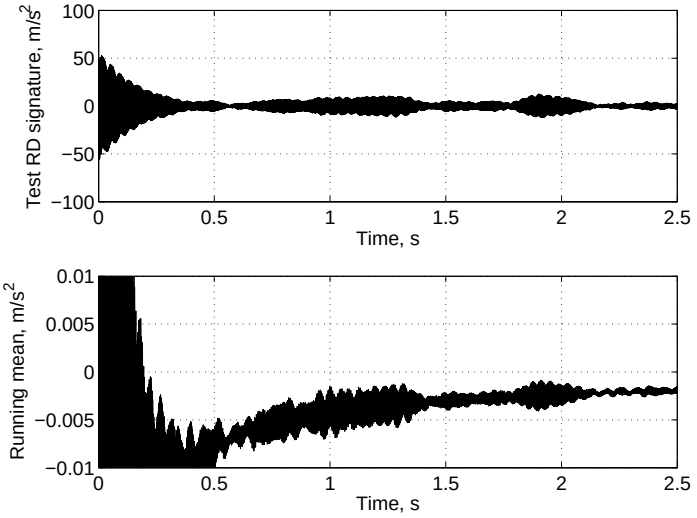

(b) RD signature and its running mean from the cracked beam.

Figure 5.11: Baseline RD signatures and their running means shown to illustrate bias, 1.75g.

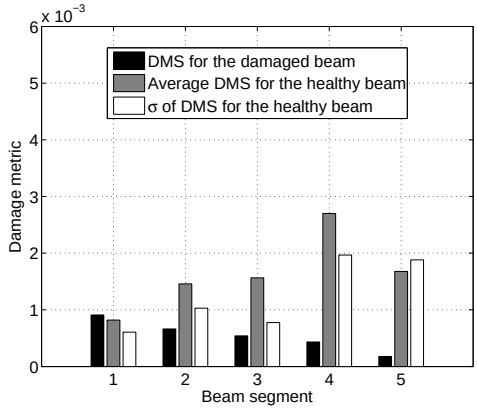

(a) Triggering level 1.5σ, signature length 2.0 s.

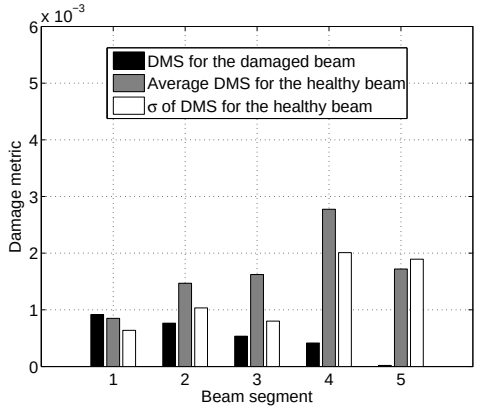

(b) Triggering level 1.5σ, signature length 2.5 s.

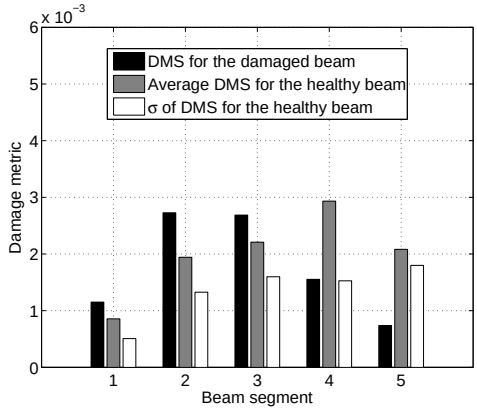

(c) Triggering level 3.0σ, signature length 2.0 s.

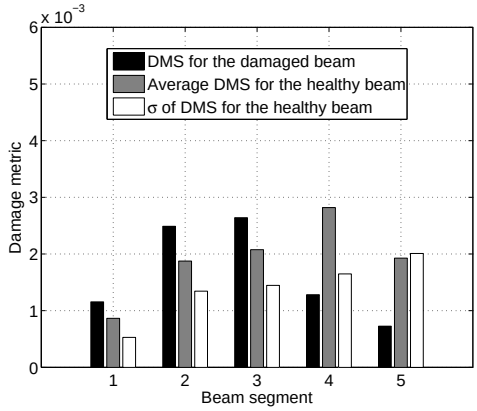

(d) Triggering level 3.0σ, signature length 2.5 s.

Figure 5.12: Detection results for 0.31g excitation level.

change in the damage metric that indicates the presence of damage is when the difference between the absolute value of the DMS criterion (black bar) and the average DMS value for the healthy system (grey bar) is greater than approximately 1.5-2 standard deviations of the DMS value for the healthy system.

From Figures 5.12 and 5.13 one can observe that the DMS criterion obtained for the damaged beam is not significantly larger than the average values and the standard deviation of that for the intact beam. In all cases shown in these figures the absolute value of the

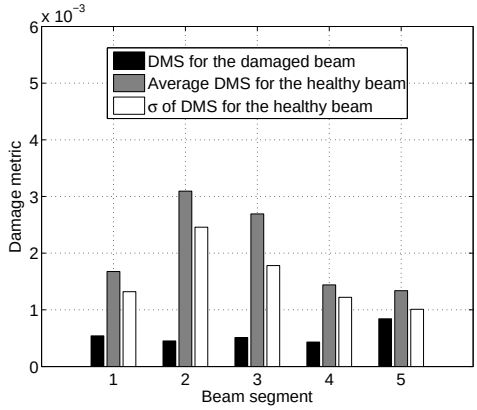

(a) Triggering level 1.5σ, signature length 2.0 s.

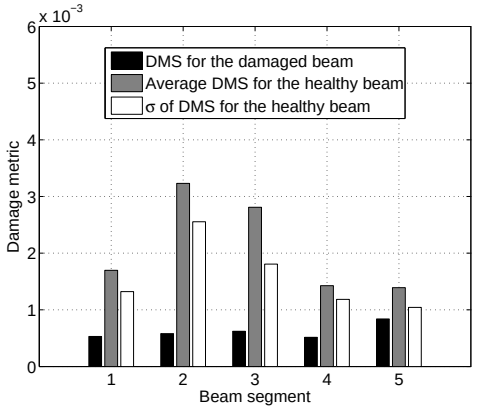

(b) Triggering level 1.5σ, signature length 2.5 s.

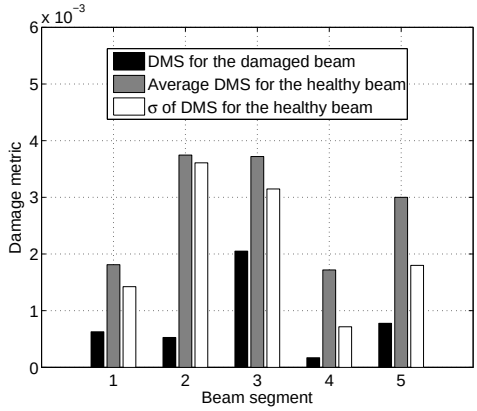

(c) Triggering level 3.0σ, signature length 2.0 s.

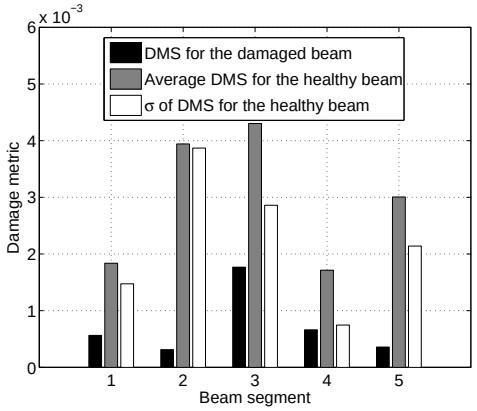

(d) Triggering level 3.0σ, signature length 2.5 s.

Figure 5.13: Detection results for 1.0g excitation level.

DMS criterion is either smaller than the average value for the healthy system, or larger than that by an amount smaller than 1 standard deviation of the DMS value for the healthy system.

From Figure 5.14 for cases with triggering level set at 3.0σ one can observe that the DMS values for segments 2 and 3 are significantly larger than the average value representing the beam in the healthy state. Hence, the method was able to detect nonlinearity due to the crack at the 1.75g excitation level.

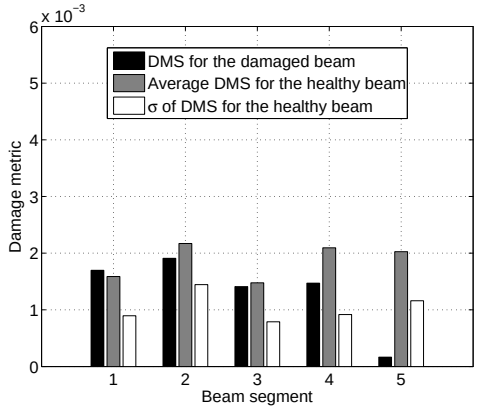

(a) Triggering level 1.5σ, signature length 2.0 s.

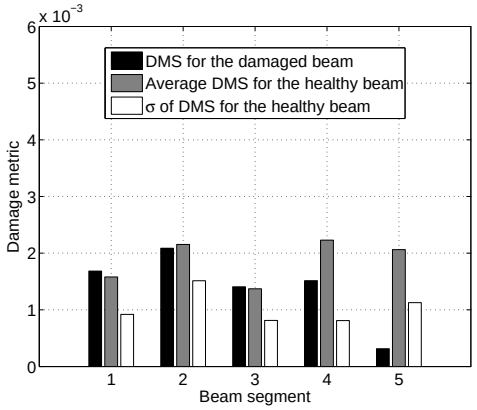

(b) Triggering level 1.5σ, signature length 2.5 s.

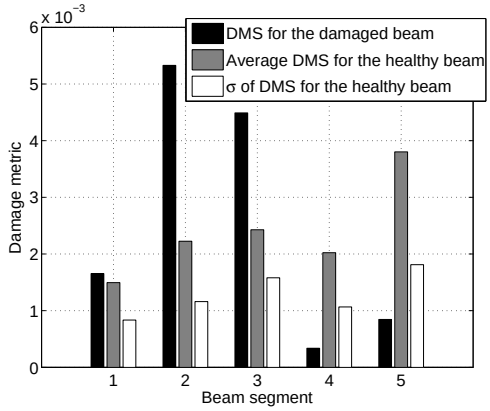

(c) Triggering level 3.0σ, signature length 2.0 s.

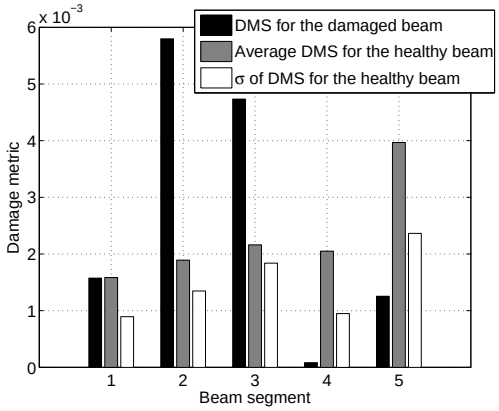

(d) Triggering level 3.0σ, signature length 2.5 s.

Figure 5.14: Detection results for 1.75g excitation level.

Figure 5.15 contains results calculated for the case with 2.45g excitation level. Clearly, for both 1.5σ and 3.0σ triggering level cases shown in Figures 5.15(a) and 5.15(b) the method failed to detect nonlinearity due to the crack. This is a counter-intuitive result because the excitation level is higher and hence the nonlinearity should be easier to observe in the response.

Recall that the experimental data at each excitation level was obtained as ten sets of 20-second long time histories. Closer examination of the data obtained at the 2.45g

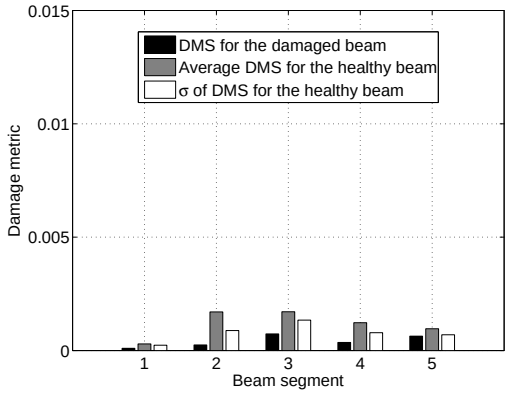

(a) Triggering level 1.5σ, signature length 2.5 s.

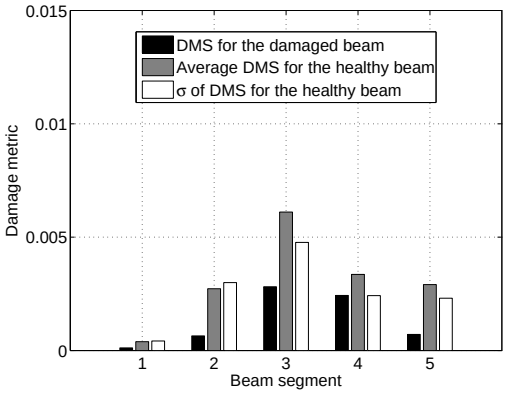

(b) Triggering level 3.0σ, signature length 2.5 s.

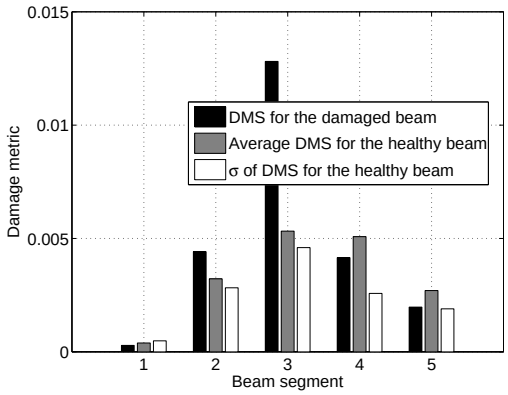

(c) Triggering level 3.0σ, signature length 2.5 s., 6 segments.

Figure 5.15: Detection results for 2.45g excitation level.

excitation level showed that if six out of ten 20-second long segments were used, then the method is able to detect the damage (see Figure 5.15(c)). There are two possible causes for this result.

1. In several recorded data segments the crack did not behave as an opening and closing crack. This may have occurred due to the roughness of the crack surfaces. In this case the beam response would remain almost linear and the DMS criterion will be close to the values corresponding to the intact beam.

2. Significant low frequency transients with the periods comparable to the length of the recorded data segments were present in the data recorded from the healthy beam. Although the recorded data is zero-meaned before calculating RD signatures, these transients distort the signatures and their statistics so that they look more like the ones from the damaged beam. This also increases the variation observed in DMS criterion for the healthy beam. Note the average value of the DMS criterion for segment 3 of the baseline beam in Figure 5.15(b) is higher than that for the same segment in Figure 5.15(c).

The second reason is supported by the finding that false alarms are produced when four 20-second long data segments obtained from the healthy beam were used as the test data. Figure 5.16 illustrates false alarms obtained in two cases. One possible explanation for the existence of these transients is that accelerometers and cables are affected by the strong electromagnetic field produced near the shaker. In fact, the signals recorded using these accelerometers were observed to be affected by electromagnetic fields during previous projects in the lab unrelated to this dissertation.

Another set of experiments was performed with the beam rotated, so that the notch with the crack was facing the ground. In this case the static loading due to gravity acted against the crack opening. Only three excitation levels were considered: 1.0g, 1.75g, and 2.45 g. As in the previous study, ten 20-second long data segments were collected for each excitation level. Signatures that are 2.0 and 2.5 seconds long were considered for the triggering level of 3.0σ.

Figure 5.17 contains results for the case with 1.0g excitation level. Clearly, the method

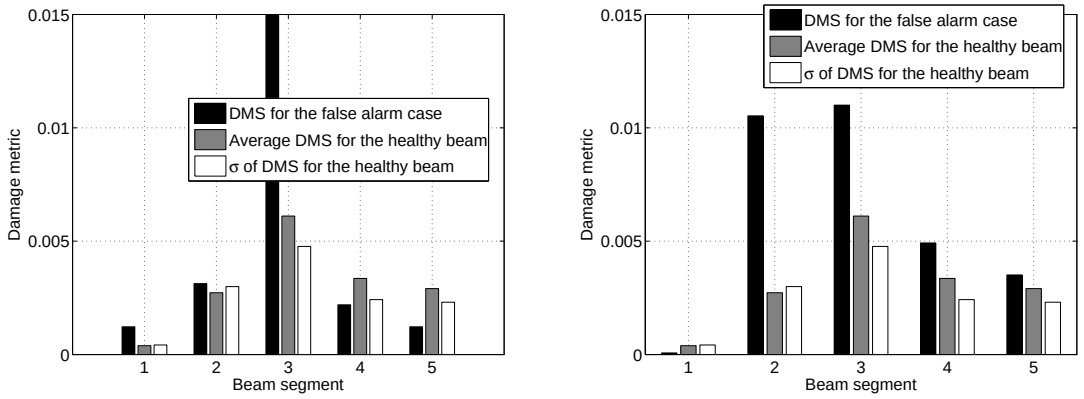

(a) False alarm case 1. Triggering level 3.0σ, signature length 2.5 s.

(b) False alarm case 2. Triggering level 3.0σ, signature length 2.5 s.

Figure 5.16: False alarms at the 2.45g excitation level.

failed to detect damage in that case. Figures 5.18 and 5.19 contain results obtained from 1.75g and 2.45g excitation cases. For both of these cases, the method fails to detect damage when all ten 20-second long data segments are used for damage detection. However, the method does indicate the presence of damage if 7 out 10 segments are utilized in the case with 1.75g excitation level, or if 4 out of 10 segments are utilized in the case with 2.45g excitation level. In Figure 5.18(c) a significant change is indicated for beam segment 3, that is indeed the segment containing the crack. In Figure 5.19(c) a significant change is indicated for beam segment 4, which is adjacent to the actual damaged segment.

Inability of the method to consistently detect damage is attributed to the two issues described earlier. Also, in this study the crack was facing down, so gravity acted against the crack opening, which may increase the likelihood of the beam behaving as a linear one, without a breathing crack.

Figure 5.20 shows the plots of the maximum damage metric and the corresponding

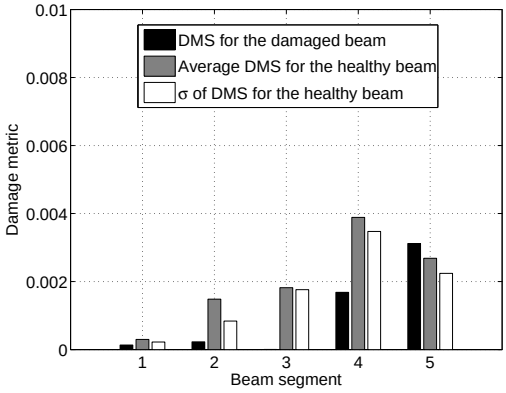

(a) Triggering level 3.0σ, signature length 2.0 s.

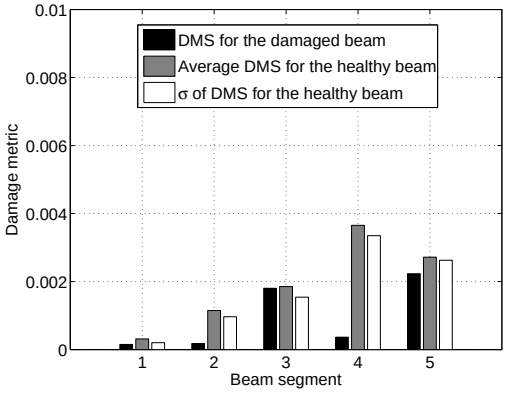

(b) Triggering level 3.0σ, signature length 2.5 s.

Figure 5.17: Detection results for 1.0g excitation level, crack facing ground.

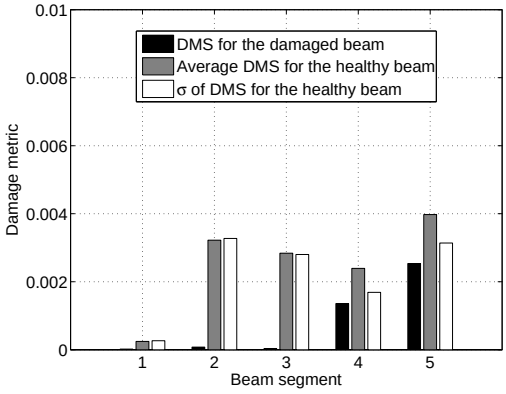

(a) Triggering level 3.0σ, signature length 2.0 s.

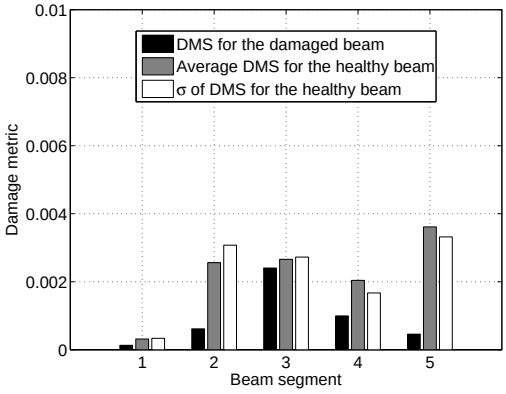

(b) Triggering level 3.0σ, signature length 2.5 s.

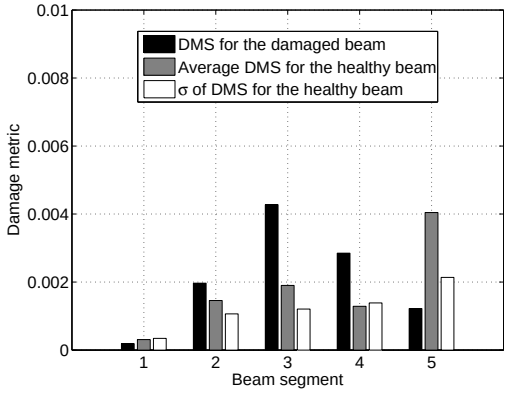

(c) Triggering level 3.0σ, signature length 2.5 s., 7 segments.

Figure 5.18: Detection results for 1.75g excitation level, crack facing ground.

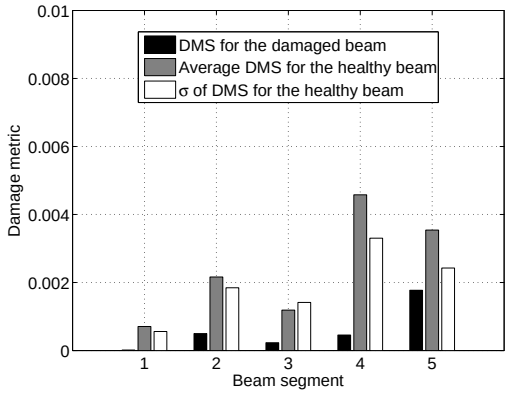

(a) Triggering level 3.0σ, signature length 2.0 s.

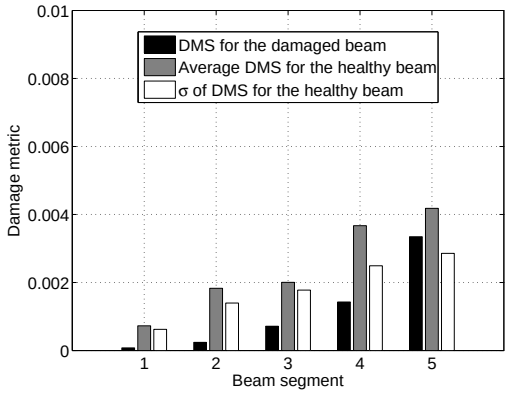

(b) Triggering level 3.0σ, signature length 2.5 s.

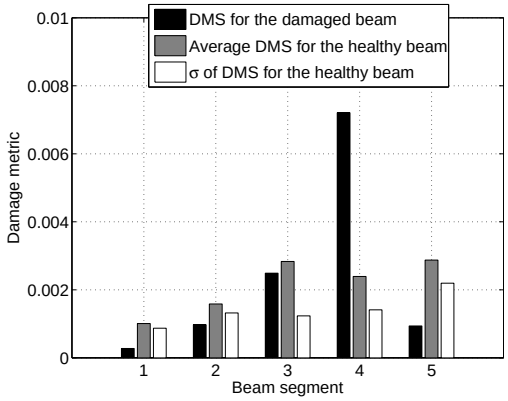

(c) Triggering level 3.0σ, signature length 2.5 s., 4 segments.

Figure 5.19: Detection results for 2.45g excitation level, crack facing ground.

average DMS value for the healthy beam with respect to excitation level. Only the data when damage was detected (except 1.0g cases) is considered to examine the changes in the damage metric with respect to excitation levels. The general trend is that the absolute value of the damage metric increases with excitation level. The DMS values obtained for 1.75g and 2.45g cases when the crack was facing upwards are higher than those for the cases when crack was facing downwards.

In the summary, it can be stated that the method is able to detect the crack in the beam

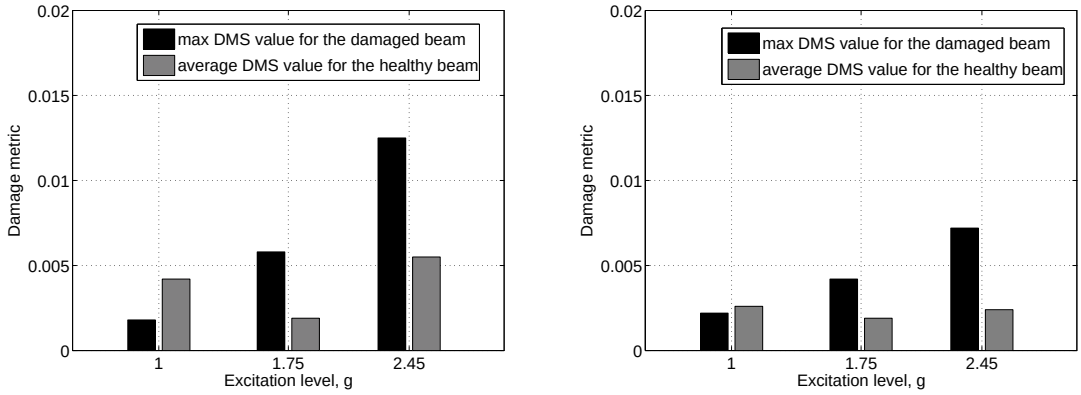

(a) Crack facing upward.

(b) Crack facing downward.

Figure 5.20: Dependence of damage metric on excitation level.

if the excitation level is high enough so that nonlinearity due to the crack will significantly affect the response. In this experimental study the method allowed to detect damage when excitation level was higher than 1.0g RMS. Location of damage is not always detected reliably, as sometimes a segment of the structure adjacent to the actual damaged segment is indicated. This correlates with the results from the study using FEM data in the previous chapter. The biggest drawback of the method is that it does not seem to perform consistently because the changes in dynamics due to nonlinearity are rather small and could be overshadowed by the transients in the sensors and data acquisition system.

Chapter 6

Summary and Conclusions

Development of the new structural health monitoring technique was presented in this work. The technique is based on detection of changes in statistics of random decrement signatures calculated from the measured response. Feature extraction includes obtaining difference signatures, which are simply the difference between the signatures of the neighboring DOFs. Utilization of difference signatures helps to make the judgement about spatial location of damage because they are supposed to represent a structural segment between the two measurement locations. Statistics representing the system in the current state are calculated from the difference signatures. Those statistics are then compared to the baseline data obtained from the system in the healthy state and a decision is made whether the stiffness change is present and where it is located.

Random decrement signatures have been utilized for damage detection in the past. The main contributions of this work to the field of structural health monitoring are listed below.

- This work investigates the use of randomdec signatures to detect the presence of nonlinearities in the response due to damage. This may allow to identify the type of damage by utilizing different statistics calculated from the signatures. This is an improvement over the previous SHM methods that utilized randomdec signatures because previous work did not consider nonlinear effects and identification of the type of damage.

- Statistical feature of randomdec signatures geared towards detection of bilinear type stiffness characteristic associated with opening and closing cracks was studied using simulation data from the FE model as well as the experimental data from a cantilever beam with a real fatigue crack.

The proposed technique and discriminating features are model-free. This is an important advantage because creating a faithful model of a realistic structure is usually a rather challenging task. In addition, since it's based on randomdec signatures it only requires output measurements and could be used on a structure excited by ambient forces that are difficult to measure.

The technique has its disadvantages as well. First, it is assumed that levels of random excitation remain constant during the service life of the structure. In reality, there may be significant variation in excitation levels. Also, the technique relies on detection of changes due to onset of nonlinear response, but it is well known that if excitation levels are small, then nonlinearity will not significantly affect the response. In such situations small amounts of damage will be difficult, if not impossible to detect.

Initial numerical study was performed on a hypothetical 5 DOF spring-mass-damper system. The damage was introduced by linear or nonlinear stiffness changes. Results showed that the standard deviation ratio test and the difference of the means test are useful for detecting and locating the damage in this hypothetical system. However, the test on the skewness statistic appeared to be ineffective because the damage did not have a significant effect the symmetry of the response distributions. The results also indicated that sensitivity of damage detection tests decreases if damaged spring element is located further away from excitation source.

The main focus of this dissertation is generation and evaluation of a new method for detection of damage due to opening and closing cracks. This type of damage usually results in a bilinear stiffness characteristic. Test on the difference of the means of the randomdec signatures is useful for detection of this type of damage. A numerical study was performed where simulated measurements were obtained from a finite element model of a frame containing a damaged member. In this study the damaged structural member possessed nonlinear stiffness characteristics. These characteristics were obtained using a detailed 3-dimensional model of the corresponding structural segment with a crack.

The results of that study showed that the new technique is able to detect crack type damage in a complex structure. It was able to highlight the damaged spar, but it was not able to precisely locate the damaged member in the spar. The results suggest that reliability of damage detection depends on the amount of noise in the measurements. If measurement data contains extremely large amounts of noise, it obscures the changes in the randomdec signatures due to onset of nonlinearity.

An additional case was considered in the study with the FE model where a smaller crack (25% cross-section deep) existed. The results indicate that the magnitude of the damage metric obtained in the damaged spar correlates with severity of the crack. Clearly, small amount of damage is more difficult to detect in the presence of noise in the measurements. Also, a case with much smaller excitation magnitude was considered for a crack that is 50% of cross-section deep. As expected, in this case reliability of detection also was shown to depend on the amount of noise present in the data.

The data from FE model simulation was also used to study the reliability of damage detection with respect to the length of the randomdec signatures and the triggering level that was used to calculate them. The results indicate that one needs to use long enough signatures so that their running mean does not fluctuate by a large amount. In this numerical study, randomdec signatures that were 3.5 seconds long were long enough so that their running mean did not vary much. In practice, to determine the desired randomdec signature length one needs to compare the running means of the signatures of different time lengths. If variation in the running mean does not reduce during the last 30% of the signature, then this can be considered an appropriate signature length. Also, the results suggest that higher triggering levels should be used since the absolute value of the damage metric tends to increase with the triggering level.

Experimental validation was performed using a cantilever beam experiment. The damaged beam used in the experiment contained a real fatigue crack instead of saw cuts that are often used to simulate damage. The technique was shown to be able to detect damage if excitation level is large enough for the nonlinearity to noticeably affect the response. For

the tested cantilever beam the technique was able to detect the damage at 1.75g and 2.45g RMS excitation levels. Location of damage is not always detected reliably, as sometimes a segment of the structure adjacent to the actual damaged segment is indicated.

Besides the dependency on excitation level, it was observed that the detection of nonlinearity due to the crack can be obstructed by the low frequency transients in the sensors' signals and data acquisition system. Also, the behavior of the crack in the damaged beam may be time dependent in the sense that it behaves as a breathing crack only during certain periods of time, while the rest of time it may remain closed due static load and surface asperities. Clearly, those issues make practical implementation of the method more difficult. Detection of breathing fatigue cracks still remains a challenging task.

An ideal SHM solution should be effective with respect to various types of anomalies that can cause both linear and nonlinear changes in dynamics. In addition, a comprehensive SHM solution should allow one to locate and classify the type of damage. The method for detection of breathing fatigue cracks studied in this work can be a part of the comprehensive SHM solution for a structure where not only it is important to detect the damage, but it is also desirable to identify the type of damage.

This technique is suitable for application in a structure subjected to strong random excitations that on average do not vary much over long periods of time and where the fault is expected to produce a strong and easily observable bilinear type nonlinearity. The study on the data from numerical simulations showed that false alarms are triggered when excitation levels of baseline and test data were an order of magnitude different. Ideally, one will collect large amounts of data for calculation of both baseline and test signatures.

These data should include time periods with both weak and strong excitations to reduce the likelihood of false alarms.

It is desirable to test the method in an experiment where sensors are less susceptible to the effects strong electromagnetic fields that may cause such issues as transients in the signals. Ideally, this can be a structure subject to ambient excitation. More sensitive statistical tests need to be developed to allow easier detection of nonlinearities. Another possible direction to achieve this goal is to attempt to utilize multiple different features for detection of damage instead of just one. The feature for detection of opening and closing cracks that was studied in this work can be a part of a comprehensive SHM solution. SHM solution utilizing several features may also allow detection of the type of damage. However, this will probably require significant amounts of empirical information about particular structure at hand in order to develop the damage classification algorithm.

References

[1] Worden, K. and Dulieu-Barton, J., "An Overview of Intelligent Fault Detection in Systems and Structures," *Structural Health Monitoring*, Vol. 3, No. 1, 2004, pp. 85–98.

[2] Doebling, S. W., Farrar, C. R., Prime, M. B., and Shevitz, D. W., "Damage Identification and Health Monitoring of Structural and Mechanical Systems from Changes in Their Vibration Characteristics: A Literature Review," Tech. Rep. LA-13070-MS, Los Alamos National Laboratory, Los Alamos, New Mexico, 87545, 1996.

[3] Doebling, S. W., Farrar, C. R., and Prime, M. B., "A Summary Review of Vibration-Based Damage Identification Methods," *Shock and Vibration Digest*, Vol. 30, No. 2, March 1998, pp. 91–105.

[4] Sohn, H., Farrar, C. R., Hemez, F. M., Shunk, D. D., Stinemates, D. W., and Nadler, B. R., "A Review of Structural Health Monitoring Literature: 1996 - 2001," Tech. Rep. LA-13976-MS, Los Alamos National Laboratory, Los Alamos, New Mexico, 87545, 2003.

[5] Carden, E. P. and Fanning, P., "Vibration Based Condition Monitoring: A Review," *Structural Health Monitoring*, Vol. 3, No. 4, December 2004, pp. 355–377.

[6] Dilena, M. and Morassi, A., "Damage Detection in Discrete Vibrating Systems," *Journal of Sound and Vibration*, Vol. 289, 2006, pp. 830–850.

[7] Bodeux, J. B. and Golinval, J. C., "Application of ARMAV models to the Identification and Damage Detection of Mechanical and Civil Engineering Structures," *Smart Materials and Structures*, Vol. 10, 2001, pp. 479–489.

[8] Kim, J.-T., Ryu, Y.-S., Cho, H.-M., and Stubbs, N., "Damage Identification In Beam-type Structures: Frequency-based Method vs Mode-Shape-based Method," *Engineering Structures*, Vol. 25, No. 1, January 2003, pp. 57–67.

[9] Humar, J., Bagchi, A., and Xu, H., "Performance of Vibration-based Techniques for the Identificaiton of Structural Damage," *Structural Health Monitoring*, Vol. 5, No. 3, September 2006, pp. 215–241.

[10] Pandey, A., Biswas, M., and Samman, M., "Damage Detection From Changes in Curvature Mode Shapes," *Journal of Sound and Vibration*, Vol. 145, No. 2, 1991, pp. 321–332.

[11] Pandey, A. and Biswas, M., "Damage Detection in Structures Using Changes in Flexibility," *Journal of Sound and Vibration*, Vol. 169, No. 1, 1994, pp. 3–17.

[12] Stubbs, N., Kim, J.-T., and Farrar, C. R., "Field Verification of a Non-Destructive Damage Localization and Severity Estimation Algorithm," *Proceedings of the* 13^{th} *International Modal Analysis Conference*, February 1995, pp. 210–218.

[13] Kaouk, M. and Zimmerman, D., "Structural Damage Assessment Using a Generalized Minimum Rank Perturbation Theory," *AIAA Journal*, Vol. 32, No. 4, April 1994, pp. 836–842.

[14] Catbas, F. N., Brown, D. L., and Aktan, A. E., "Parameter Estimation for Multiple-Input Multiple-Output Modal Analysis of Large Structures," *Journal of Engineering Mechanics*, Vol. 130, No. 8, August 2004, pp. 921–930.

[15] Sohn, H., Dzwonczyk, M., Straser, E. G., Law, K. H., Meng, T., and Kiremidjian, A. S., "Adaptive Modeling of Environmental Effects in Modal Parameters for Damage Detection in Civil Structures," *Proceedings of SPIE, Smart Systems for Bridges, Structures, and Highways*, Vol. 3325, 1998, pp. 127–138.

[16] Bedewi, N. E. and Yang, J. C. S., "A System Identification Technique Based on the Random Decrement Signatures. Part 2: Experimental Results." *Proceedings of the* 58^{th} *Shock and Vibration Symposium*, Vol. 1, October 1987, pp. 275–287.

[17] Siringoringo, D. M. and Fujino, Y., "Experimental Study of Laser Doppler Vibrometer and Ambient Vibration For Vibration-based Damage Detection," *Engineering Structures*, Vol. 28, No. 13, November 2006, pp. 1803–1815.

[18] Juang, J.-N. and Pappa, R. S., "An Eigensystem Realization Algorithm For Modal Parameter Identification and Model Reduction," *AIAA Journal of Guidance, Control, and Dynamics*, Vol. 8, No. 5, 1985, pp. 620–627.

[19] Worden, K., "Structural Fault Detection Using a Novelty Measure," *Journal of Sound and Vibration*, Vol. 201, No. 1, 1997, pp. 85–101.

[20] Masri, S. F., Smyth, A. W., Chassiokis, A. G., Caughey, T. K., and Hunter, N. F., "Application of Neural Networks For Detection of Changes in Nonlinear Systems," *Journal of Engineering Mechanics*, Vol. 126, No. 7, July 2000, pp. 666–676.

[21] Zapico, J. L., Worden, K., and Molina, F. J., "Vibration-based Damage Assessment in Steel Frames Using Neural Networks," *Smart Materials and Structures*, Vol. 10, 2001, pp. 553–559.

[22] Yeung, W. and Smith, J., "Damage Detection In Bridges Using Neural Networks For Pattern Recognition of Vibration Signatures," *Engineering Structures*, Vol. 27, No. 5, April 2005, pp. 685–698.

[23] Worden, K., Manson, G., and Allman, D., "Experimental Validation of a Structural Health Monitoring Methodology: Part 1. Novelty Detection on a Laboratory Structure," *Journal of Sound and Vibration*, Vol. 259, No. 2, 2003, pp. 323–343.

[24] Manson, G., Worden, K., and Allman, D., "Experimental Validation of a Structural Health Monitoring Methodology: Part 2. Novelty Detection on a GNAT Aircraft," *Journal of Sound and Vibration*, Vol. 259, No. 2, 2003, pp. 345–363.

[25] Manson, G., Worden, K., and Allman, D., "Experimental Validation of a Structural Health Monitoring Methodology: Part 3. Damage Location on an Aircraft Wing," *Journal of Sound and Vibration*, Vol. 259, No. 2, 2003, pp. 365–385.

[26] Crupi, V., Guglielmino, E., and Milazzo, G., "Neural-Network-Based System For Novel Fault Detection in Rotating Machinery," *Journal of Vibration and Control*, Vol. 10, No. 8, August 2004, pp. 1137–1150.

[27] Hunter, N. F., "Bilinear System Characterization from Nonlinear Time Series Analysis," *Proceedings of the* 17^{th} *International Modal Analysis Conference*, Vol. 2, February 1999, pp. 1488–1494.

[28] Epureanu, B. I. and Yin, S.-H., "Identification of Damage in an Aeroelastic System Based on Attractor Deformations," *Computers and Structures*, Vol. 82, 2004, pp. 2743–2751.

[29] Adams, D. E. and Nataraju, M., "A Nonlinear Dynamical Systems Framework for Structural Diagnosis and Prognosis," *International Journal of Engineering Science*, Vol. 40, 2002, pp. 1919–1941.

[30] Brown, R. L. and Adams, D. E., "Equilibrium Point Damage Prognosis Models for Structural Health Monitoring," *Journal of Sound and Vibration*, Vol. 262, 2003, pp. 591–611.

[31] Nichols, J., Virgin, L. N., Todd, M. D., and Nichols, J., "On the Use of Attractor Dimension as a Feature in Structural Health Monitoring," *Mechanical Systems and Signal Processing*, Vol. 17, No. 6, 2003, pp. 1305–1320.

[32] Nichols, J., Todd, M. D., Seaver, M., and Virgin, L. N., "Use of Chaotic Excitation and Attractor Property Analysis in Structural Health Monitoring," *Physical Reviews*, Vol. E 67, No. 016209, 2003.

[33] Moniz, L., Nichols, J., Nichols, C. J., Seaver, M., Trickey, S. T., Todd, M. D., Pecora, L. M., and Virgin, L. N., "A Multivariate, Attractor-Based Approach to Structural Health Monitoring," *Journal of Sound and Vibration*, Vol. 283, 2005, pp. 295–310.

[34] Todd, M. D., Erickson, K., Chang, L., Lee, K., and Nichols, J. M., "Using Chaotic Interrogation and Attractor Nonlinear Cross-Prediction to Detect Fastener Preload Loss in an Aluminum Frame," *Chaos*, Vol. 14, No. 2, June 2004, pp. 387–399.

[35] Chen, G., Yang, X., Ying, X., and Nanni, A., "Damage Detection of Concrete Beams Using Nonlinear Features of Forced Vibration," *Structural Health Monitoring*, Vol. 5, No. 2, June 2006, pp. 125–141.

[36] Wang, S., Ren, Q., and Qiao, P., "Structural Damage Detection Using Local Damage Factor," *Journal of Vibration and Control*, Vol. 12, No. 9, September 2006, pp. 955–973.

[37] Mickens, T., Schulz, M., Sundaresan, M., and Ghoshal, A., "Structural Health Monitoring of an Aircraft Joint," *Mechanical Systems and Signal Processing*, Vol. 17, No. 2, 2003, pp. 285–303.

[38] Park, G., Rutherford, A. C., Sohn, H., and Farrar, C. R., "An Outlier Analysis Framework for Impedance-Based Structural Health Monitoring," *Journal of Sound and Vibration*, Vol. 286, 2005, pp. 229–250.

[39] Park, G., Kabeya, K., Cudney, H., and Inman, D. J., "Impedance-Based Structural Health Monitoring for Temperature Varying Applications," *JSME International Journal*, Vol. 42, No. 2, 1999, pp. 249–258.

[40] Mal, A., Ricci, F., Banerjee, S., and Shih, F., "A Conceptual Structural Health Monitoring System Based on Vibration and Wave Propagation," *Structural Health Monitoring*, Vol. 4, No. 3, 2005, pp. 283–293.

[41] Rizzo, P. and Lanza di Scalea, F., "Feature Extraction For Defect Detection in Strands by Guided Ultrasonic Waves," *Structural Health Monitoring*, Vol. 5, No. 3, 2006, pp. 297–308.

[42] Sawyer, J. P. and Rao, S. S., "Structural Fault Detection Using Fuzzy Logic," *Proceedings of the AIAA Dynamics Specialists Conference*, April 1996, pp. 214–222.

[43] Sampaio, R. P. C., Maia, N. M. M., and Silva, J. M. M., "Damage Detection Using Frequency-Response-Function Curvature Method," *Journal of Sound and Vibration*, Vol. 226, No. 5, 1999, pp. 1029–1042.

[44] Ismail, Z., Razak, H., and Rahman, A., "Determination of Damage Location In RC Beams Using Mode Shape Derivatives," *Engineering Structures*, Vol. 28, No. 11, September 2006, pp. 1566–1573.

[45] Maia, N. M. M., Silva, J. M. M., Almas, E. A. M., and Sampaio, R. P. C., "Damage Detection in Structures: From Mode Shape to Frequency Response Function Methods," *Mechanical Systems and Signal Processing*, Vol. 17, No. 3, 2003, pp. 489–498.

[46] Sohn, H., Allen, D. W., Worden, K., and Farrar, C. R., "Structural Damage Classification Using Extreme Value Statistics," *Journal of Dynamic Systems, Measurement, and Control*, Vol. 127, March 2005, pp. 125–132.

[47] Sohn, H. and Law, K. H., "Damage Diagnosis Using Experimental Ritz Vectors," *Journal of Engineering Mechanics*, Vol. 127, No. 11, November 2001, pp. 1184–1193.

[48] Castro, E., Garcia-Hernandez, M., and Gallebo, A., "Damage Detection in Rods by Means of the Wavelet Analysis of Vibrations: Influence of the Mode Order," *Journal of Sound and Vibration*, Vol. 296, No. 4-5, October 2006, pp. 1028–1038.

[49] Reda Taha, M., Noureldin, A., Lucero, J., and Baca, T., "Wavelet Transform for Structural Health Monitoring: A Compendium of Uses and Features," *Structural Health Monitoring*, Vol. 5, No. 3, September 2006, pp. 267–295.

[50] Vanlanduit, S., Verboven, P., and Guillaume, P., "On-line Detection of Fatigue Cracks Using an Automatic Mode Tracking Technique," *Journal of Sound and Vibration*, Vol. 266, 2003, pp. 805–814.

[51] Yang, J. N., Lei, Y., Lin, S., and Huang, N., "Hilbert-Huang Based Approach for Structural Damage Detection," *Journal of Engineering Mechanics*, Vol. 130, No. 1, 2004, pp. 85–95.

[52] Cole, H. A., *Failure Detection of a Space Shuttle Wing by Random Decrement*, NASA TMX-62041, 1971.

[53] Cole, H. A., *Method and Apparatus for Measuring the Damping Characteristics of a Structure*, United States Patent No. 3,620,069, November 16, 1971.

[54] Cole, H. A., *On-Line Failure Detection and Damping Measurements of Aerospace Structures By Random Decrement Signature*, NASA CR-2205, 1973.

[55] Cole, H. A., "On-The-Line Analysis of Random Vibrations," *AIAA paper No. 68-288*, 1968.

[56] Asmussen, J. C., *Modal Analysis Based on the Random Decrement Technique - Application to Civil Engineering Structures*, Ph. d. dissertation, Univesity of Aalborg, Department of Building Technology and Structural Engineering, Sohngaardholmsvej 57, 9000 Aalborg, Denmark, August 1997.

[57] Ibrahim, S. R., "Random Decrement Technique for Modal Identification of Structures," *Journal of Spacecraft and Rockets*, Vol. 14, No. 11, November 1977, pp. 696–700.

[58] Cho, K. P., Tamura, Y., Itoh, T., Narikawa, M., Uchikawa, Y., Nishimura, I., and Ohshima, Y., "Field Measurement of Damping in Industrial Chimneys and Towers," *Structural Engineering and Mechanics*, Vol. 12, No. 4, 2001, pp. 449–457.

[59] Asmussen, J. C., Ibrahim, S. R., and Brincker, R., "Random Decrement and Regression Analysis of Traffic Response of Bridges," *Proceedings of the* 14^{th} *International Modal Analysis Conference*, Vol. 1, 1996, pp. 453–458.

[60] Asmussen, J. C. and Brincker, R., "Estimation of Frequency Response Functions by Random Decrement," *Proceedings of the* 14^{th} *International Modal Analysis Conference*, 1996, pp. 246–252.

[61] Yang, J. C. S., Chen, J., and Dagalakis, N. G., "Damage Detection in Offshore Structures by the Random Decrement Technique," *ASME Journal of Energy Resources Technology*, Vol. 106, March 1984, pp. 38–42.

[62] Tsai, T., Yang, J. C. S., and Chen, R. Z., "Detection of Damages in Structures by the Cross Random Decrement Technique," *Proceedings of the* 3^{rd} *International Modal Analysis Conference*, Orlando, FL, January 1985, pp. 691–700.

[63] Bedewi, N. E. and Yang, J. C. S., "A System Identification Technique Based on the Random Decrement Signatures. Part 1: Theory and Simulation." *Proceedings of the* 58^{th} *Shock and Vibration Symposium*, Vol. 1, October 1987, pp. 257–273.

[64] Zubaydi, A., Haddara, M. R., and Swamidas, A. S. J., "Random Decrement Technique for Damage Identification of Stiffened Plates," 18^{th} *International Modal Analysis Conference*, San Antonio, TX, USA, 2000, pp. 1399–1405.

[65] Zubaydi, A., Haddara, M. R., and Swamidas, A. S. J., "Damage Identification in a Ship's Structure Using Neural Networks," *Ocean Engineering*, Vol. 29, No. 10, August 2002, pp. 1187–1200.

[66] Li, H. C. H., Weis, M., Herszberg, I., and Mouritz, A. P., "Damage Detection in a Fibre Reinforced Composite Beam Using Random Decrement Signatures," *Composite Structures*, Vol. 66, 2004, pp. 159–167.

[67] The MathWorks Inc., 3 Apple Hill Drive, Natick, MA 01760, *Using MATLAB*, July 2002.

[68] Sundaresan, M., Ghoshal, A., Li, J., Schulz, M., Pai, P. F., and Chung, J. H., "Experimental Damage Detection on a Wing Panel Using Vibration Defelction Shapes," *Structural Health Monitoring*, Vol. 2, No. 3, September 2003, pp. 243–256.

[69] Ritdumrongkul, S. and Fujino, Y., "Identification of the Location and Size of Cracks in Beams by a Piezoceramic Actuator-Sensor," *Structural Control and Health Monitoring*, Vol. 14, No. 6, October 2007, pp. 931–943.

[70] Nikolakopoulos, P., Katsareas, D., and Papadopoulos, C., "Crack Identification in Frame Structures," *Computers and Structures*, Vol. 64, No. 1-4, 1997, pp. 389–406.

[71] Narayana, L. K. and Jebaraj, C., "Sensitivity Analysis of Local/Global Modal Parameters For Identification of a Crack in a Beam," *Journal of Sound and Vibration*, Vol. 228, No. 5, December 1999, pp. 977–994.

[72] Xiang, J., Chen, X., Li, B., He, Y., and He, Z., "Identification of a Crack in a Beam Based on the Finite Element Method of a B-Spline Wavelet on the Interval," *Journal of Sound and Vibration*, Vol. 296, No. 4-5, October 2006, pp. 1046–1052.

[73] Pai, P. F., Young, L. G., and Lee, S.-Y., "A Dynamics-based Method for Crack Detection and Estimation," *Structural Health Monitoring*, Vol. 2, No. 1, January 2003, pp. 5–25.

[74] Kim, J.-T. and Stubbs, N., "Crack Detection in Beam-type Structures Using Frequency Data," *Journal of Sound and Vibration*, Vol. 259, No. 1, January 2003, pp. 145–160.

[75] Law, S. and Lu, Z., "Crack Identification in Beam From Dynamic Responses," *Journal of Sound and Vibration*, Vol. 285, No. 4-5, August 2005, pp. 967–987.

[76] Patil, D. and Maiti, S., "Experimental Verification of a Method of Detection of Multiple Cracks in Beams Based on Frequency Measurements," *Journal of Sound and Vibration*, Vol. 281, No. 1-2, March 2005, pp. 439–451.

[77] Hillis, A., Neild, S., Drinkwater, B., and Wilcox, P., "Global Crack Detection Using Bispectral Analysis," *Proceedins of the Royal Society A: Mathematical, Physical and Engineering Sciences*, Vol. 462, No. 2069, May 2006, pp. 1515 – 1530.

[78] Ryue, J. and White, P., "The Detection of Cracks in Beams Using Chaotic Excitations," *Journal of Sound and Vibration*, Vol. 307, No. 3-5, November 2007, pp. 627–638.

[79] Peng, Z. K., Lang, Z. Q., and Billings, S. A., "Crack Detection Using Nonlinear Output Frequency Response Functions," *Journal of Sound and Vibration*, Vol. 301, January 2007, pp. 777–788.

[80] Chondros, T. G., Dimarogonas, A. D., and Yao, J., "Vibration of a Beam with a Breathing Crack," *Journal of Sound and Vibration*, Vol. 239, No. 1, January 2001, pp. 57–67.

[81] Sundermeyer, J. and Weaver, R., "On Crack Identification and Characterization in a Beam by Non-linear Vibration Analysis," *Journal of Sound and Vibration*, Vol. 183, No. 5, 1995, pp. 857–871.

[82] Luzzato, E., "Approximate Computation of Nonlinear Effects In a Vibrating Cracked Beam," *Journal of Sound and Vibration*, Vol. 265, August 2003, pp. 745–763.

[83] Bovsunovsky, A. P. and Matveev, V. V., "Analytical Approach to the Determination of Dynamic Characteristics of a Beam with a Closing Crack," *Journal of Sound and Vibration*, Vol. 235, No. 3, August 2000, pp. 415–434.

[84] Tsyfansky, S. and Beresnevich, V., "Non-linear Vibration Method For Detection of Fatigue Cracks in Aircraft Wings," *Journal of Sound and Vibration*, Vol. 236, No. 1, September 2000, pp. 49–60.

[85] Hibbitt, Karlsson & Sorensen, Inc., 1080 Main Street, Pawtucket, RI 02860-4847, *ABAQUS/CAE/Standard/Explicit User's Manual, Version 6.4*, 2003.

[86] Dimarogonas, A. D., "Vibration of Cracked Structures: A State of the Art Review," *Engineering Fracture Mechanics*, Vol. 55, No. 5, 1996, pp. 831–857.

[87] Friswell, M. I. and Penny, J. E. T., "Crack Modeling for Structural Health Monitoring," *Structural Health Monitoring*, Vol. 1, No. 2, 2002, pp. 139–148.